

ENERGY STABLE AND MOMENTUM CONSERVING HYBRID FINITE ELEMENT METHOD FOR THE INCOMPRESSIBLE NAVIER–STOKES EQUATIONS

ROBERT JAN LABEUR* AND GARTH N. WELLS†

Abstract. A hybrid method for the incompressible Navier–Stokes equations is presented. The method inherits the attractive stabilizing mechanism of upwinded discontinuous Galerkin methods when momentum advection becomes significant, equal-order interpolations can be used for the velocity and pressure fields, and mass can be conserved locally. Using continuous Lagrange multiplier spaces to enforce flux continuity across cell facets, the number of global degrees of freedom is the same as for a continuous Galerkin method on the same mesh. Different from our earlier investigations on the approach for the Navier–Stokes equations, the pressure field in this work is discontinuous across cell boundaries. It is shown that this leads to very good local mass conservation and, for an appropriate choice of finite element spaces, momentum conservation. Also, a new form of the momentum transport terms for the method is constructed such that global energy stability is guaranteed, even in the absence of a point-wise solenoidal velocity field. Mass conservation, momentum conservation and global energy stability are proved for the time-continuous case, and for a fully discrete scheme. The presented analysis results are supported by a range of numerical simulations.

Key words. Finite element method; hybrid finite element methods; incompressible Navier–Stokes equations.

AMS subject classifications. 65N12, 65N30, 76D05, 76D07.

1. Introduction. A method that combines attractive features of discontinuous and continuous Galerkin finite element methods for the incompressible Navier Stokes equations was presented in Labeur and Wells [1] and further extended to the case of moving domains and free-surface flows in Labeur and Wells [2]. The method incorporated naturally the evaluation of upwinded advective fluxes on cell facets, in the same spirit as discontinuous Galerkin methods, thereby stabilizing flows with significant momentum advection, and it is possible to use equal-order polynomial bases for the velocity and pressure components. However, the number of global degrees of freedom on a given mesh is the same as for a continuous Galerkin method using the same polynomial orders. The issue regarding the significantly greater number of global degrees of freedom for low- to moderate-order discontinuous Galerkin methods compared to continuous Galerkin methods is thus circumvented. However, the method in [1] was restricted to continuous pressure fields, and it could not be proven that the method is globally energy stable. These short-comings are addressed in this paper, with a formulation presented that permits discontinuous pressure fields, is globally energy stable, conserves momentum and has excellent local mass conservation properties.

The key to the methodology that we present for constructing schemes is the postulation of cell-wise balances, subject to weakly enforced boundary conditions. The boundary condition to be satisfied (weakly) is provided by a function that lives on cell facets only. An equation for this extra field is furnished by insisting on weak continuity of the associated ‘numerical’ flux. The concept of weak enforcement of flux continuity across cell facets is central in hybridized finite element methods (for an overview see [3]). A feature of these methods is that functions on cells are linked

*Faculty of Civil Engineering and Geosciences, Delft University of Technology, Stevinweg 1, 2628 CN Delft, The Netherlands (r.j.labeur@tudelft.nl)

†Department of Engineering, University of Cambridge, Trumpington Street, Cambridge CB2 1PZ, United Kingdom (gnw20@cam.ac.uk)

to functions on neighboring cells *only* via functions that live on cell facets, and not directly via the flux terms. Therefore, functions on cells can be eliminated locally in favor of the functions that live on cell facets only (via static condensation), thus reducing the number of globally coupled degrees of freedom. If the functions enforcing the continuity of the fluxes, and which live only on cell facets, are discontinuous, then point-wise continuous fluxes can be obtained for suitably chosen function spaces. In contrast, in our method we advocate the use of facet functions that are continuous, which leads to a significant reduction in the number of globally coupled degrees of freedom, since the local elimination procedure will lead to a global problem of the same size as a corresponding continuous Galerkin method. Yet, it is straightforward to demonstrate local momentum and mass conservation, in terms of the numerical fluxes, as is typical of discontinuous Galerkin methods. Also the stabilizing mechanism of the flux formulation, involving the advection terms and the pressure-velocity coupling, are directly inherited from the discontinuous Galerkin method and lead to favorable stability properties.

We are not alone in considering methods that draw on both discontinuous and continuous Galerkin methods. Hughes et al. [4] developed a method for the advection-diffusion equation, and the formulation in [1] for the advection-diffusion equation reduces to that of Hughes et al. [4] in the advective limit. In the diffusive case, there is a subtle difference, with the diffusive flux in Hughes et al. [4] being upwinded, whereas a centered approach is used in Labeur and Wells [1]. Simulations using the approach for the advection-diffusion equation exhibited very good stability properties, minimal dissipation and standard convergence rates. For the case of the linear advection-diffusion-reaction equation, stability (via an inf-sup condition) and convergence at a rate of $k + 1$ in the diffusive limit and $k + 1/2$ in the advective limit was later proved [5]. In the context of hybridized methods, Cockburn and co-workers have published a number of works (e.g. [6, 7]) that share features with the methodology that we consider. A hybrid field on cell interfaces is presented in Egger and Schöberl [8] for the advection-diffusion problem. Güzey et al. [9] present a hybrid continuous-discontinuous finite element method for elliptic problems, coined embedded discontinuous Galerkin method, which is conceptually related to the method in Labeur and Wells [1].

The method formulated and analyzed in this work is an extension of the method presented in Labeur and Wells [1] for the advection-diffusion equation and for the incompressible Navier-Stokes equations. Unlike in our previous efforts [1, 2], we consider here pressure fields that are discontinuous across cell facets. The impact of this on the local (cell-wise) mass conservation properties of the method is demonstrated. Another feature that distinguishes the formulation developed in this work from our earlier work for the Navier-Stokes equations is the use of a skew-symmetric form of the advective term. The derivation of the skew-symmetric formulation is not trivial in the considered setting, but it is shown that it brings the advantage of guaranteeing stability in terms of the total kinetic energy, even when the velocity field is not point-wise solenoidal. The combination of discontinuous pressure fields and skew-symmetric advection terms leads to a method that for equal-order basis functions preserves mass and momentum and is also stable in terms of the total kinetic energy. The analysis results that we present are supported by a number of computations for both the Stokes and incompressible Navier-Stokes equations. The computer code necessary to reproduce all examples presented in this work is available in the supporting material [10] under a GNU public license.

The remainder of this work is structured as follows. We first define concretely the problem of interest, and then develop a semi-discrete finite element formulation. Some properties of the semi-discrete problem are then analyzed. This is followed by a particular fully-discrete formulation, and it is shown that the considered properties of the semi-discrete problem are inherited by the fully discrete problem. This is followed by numerical examples, after which conclusions are drawn.

2. Incompressible Navier–Stokes equations. We consider a domain of interest $\Omega \subset \mathbb{R}^d$, where $1 \leq d \leq 3$ is the spatial dimension. The boundary $\partial\Omega$ is assumed sufficiently smooth and the outward unit normal vector on $\partial\Omega$ is denoted by \mathbf{n} . The boundary is partitioned such that $\Gamma_D \cap \Gamma_N = \partial\Omega$ and $\Gamma_D \cup \Gamma_N = \emptyset$. The time interval of interest is $I = (0, t_N]$.

The non-dimensional incompressible Navier–Stokes problem on $\Omega \times I$ reads: given the viscosity ν , the forcing term $\mathbf{f}: \Omega \times I \rightarrow \mathbb{R}^d$, the momentum flux $\mathbf{h}: \Gamma_N \times I \rightarrow \mathbb{R}^d$ and the solenoidal initial condition $\mathbf{u}_0: \Omega \rightarrow \mathbb{R}^d$, find the velocity field $\mathbf{u}: \Omega \times I \rightarrow \mathbb{R}^d$ and the pressure field $p: \Omega \times I \rightarrow \mathbb{R}$ such that

$$\frac{\partial \mathbf{u}}{\partial t} + \nabla \cdot \boldsymbol{\sigma} = \mathbf{f} \quad \text{on } \Omega \times I, \quad (2.1)$$

$$\boldsymbol{\sigma} = p\mathbf{I} - 2\nu\nabla^s \mathbf{u} + \mathbf{u} \otimes \mathbf{u} \quad \text{on } \Omega \times I, \quad (2.2)$$

$$\nabla \cdot \mathbf{u} = 0 \quad \text{on } \Omega \times I, \quad (2.3)$$

$$\mathbf{u} = \mathbf{0} \quad \text{on } \Gamma_D \times I, \quad (2.4)$$

$$\boldsymbol{\sigma} \mathbf{n} - \max(\mathbf{u} \cdot \mathbf{n}, 0) \mathbf{u} = \mathbf{h} \quad \text{on } \Gamma_N \times I, \quad (2.5)$$

$$\mathbf{u}(\mathbf{x}, 0) = \mathbf{u}_0(\mathbf{x}) \quad \text{on } \Omega, \quad (2.6)$$

where $\boldsymbol{\sigma}$ is the momentum flux, \mathbf{I} is the identity tensor, $\nabla^s \mathbf{u} = (\nabla \mathbf{u} + \nabla \mathbf{u}^T)/2$ is the symmetric gradient, in which $[\nabla \mathbf{u}]_{ij} = \partial u_i / \partial x_j$, and $[\mathbf{u} \otimes \mathbf{u}]_{ij} = u_i u_j$. The Neumann boundary condition has been formulated such that on portions of Γ_N on which $\mathbf{u} \cdot \mathbf{n} < 0$ (inflow boundaries) the total momentum flux is prescribed, while on portions of Γ_N on which $\mathbf{u} \cdot \mathbf{n} \geq 0$ (outflow boundaries) only the diffusive part of the momentum flux is prescribed.

3. Finite element method. The hybrid finite element method is defined in this section. The essence of the method is posing all balance equations cell-wise in a weak sense, with a suitably constructed numerical flux, and complementing the cell-wise balance laws by a global equation enforcing weak continuity of the numerical flux across cell facets.

3.1. Definitions. We consider a triangulation \mathcal{T} of the domain Ω into open, non-overlapping sub-domains K (cells). The outward unit normal vector on the boundary ∂K of each cell is denoted by \mathbf{n} . Adjacent cells share a common facet F , and $\mathcal{F} = \bigcup F$ is the union of all facets, including the exterior boundary facets. A measure of the size of a cell K is denoted by h_K . When evaluated on a shared facet, h_K is used to imply the average cell size measure of the adjacent cells.

Consider first the vector finite element spaces V_h and \bar{V}_h :

$$V_h := \left\{ \mathbf{v}_h \in [L^2(\mathcal{T})]^d, \mathbf{v}_h \in [P_k(K)]^d \quad \forall K \in \mathcal{T} \right\}, \quad (3.1)$$

$$\bar{V}_h := \left\{ \bar{\mathbf{v}}_h \in [L^2(\mathcal{F})]^d, \bar{\mathbf{v}}_h \in [P_{\bar{k}}(F)]^d \quad \forall F \in \mathcal{F}, \bar{\mathbf{v}}_h = \mathbf{0} \text{ on } \Gamma_D \right\}, \quad (3.2)$$

where $P_k(K)$ denotes the space of Lagrange polynomials on K of order $k > 0$, and $P_{\bar{k}}(F)$ denotes the space of Lagrange polynomials on F of order $\bar{k} \geq 0$. The space V_h

contains vector-valued functions that are discontinuous across cell boundaries, while functions in \bar{V}_h are defined on cell facets only. Furthermore, functions in \bar{V}_h satisfy the homogeneous Dirichlet boundary condition on Γ_D . Scalar finite element spaces Q_h and \bar{Q}_h are defined by:

$$Q_h := \{q_h \in L^2(\mathcal{T}), q_h \in P_m(K) \ \forall K \in \mathcal{T}\}, \quad (3.3)$$

$$\bar{Q}_h := \{\bar{q}_h \in L^2(\mathcal{F}), \bar{q}_h \in P_{\bar{m}}(F) \ \forall F \in \mathcal{F}\}, \quad (3.4)$$

where the polynomial orders $m \geq 0$ and $\bar{m} \geq 0$. Mirroring the vector spaces, Q_h contains functions that are discontinuous across cell facets, while functions in \bar{Q}_h are defined on cell facets only.

For algorithmic reasons, it may be advantageous to compute with the finite element spaces

$$\bar{V}_h^* := \bar{V}_h \cap [H^1(\mathcal{F})]^d, \quad (3.5)$$

$$\bar{Q}_h^* := \bar{Q}_h \cap H^1(\mathcal{F}), \quad (3.6)$$

in place of \bar{V}_h and \bar{Q}_h , respectively, using polynomial orders $\bar{k} \geq 1$ and $\bar{m} \geq 1$. This will be discussed in Section 6, and all computational results presented in Section 7 will employ facet functions that are continuous.

3.2. Semi-discrete weak local/global balances. We formulate now a semi-discrete finite element problem by considering what we will refer to as ‘local’ and ‘global’ equations. The ‘local’ equations solve the problem cell-wise in which the velocity and pressure boundary conditions are provided by auxiliary fields that live on cell facets only. To determine the fields that live on cell facets, ‘global’ equations are formulated by requiring weak continuity of the mass and momentum fluxes across element interfaces. The methodology behind the construction of the formulation is elucidated by presenting a collection of Galerkin problems for the various balances, after which the considered Galerkin finite element problem is completely and formally defined.

3.2.1. Local/global continuity equation. A Galerkin approximation of the incompressibility constraint (2.3) in a cell-wise fashion requires that the approximate velocity $\mathbf{u}_h \in V_h$ satisfies

$$\sum_K \int_K \mathbf{u}_h \cdot \nabla q_h \, dx - \sum_K \int_{\partial K} \hat{\mathbf{u}}_h \cdot \mathbf{n} \, q_h \, ds = 0 \quad \forall q_h \in Q_h, \quad (3.7)$$

where $\hat{\mathbf{u}}_h$ is the ‘numerical’ mass flux on ∂K , and is chosen to be

$$\hat{\mathbf{u}}_h = \mathbf{u}_h - \frac{\beta h_K}{\nu + 1} (\bar{p}_h - p_h) \mathbf{n}, \quad (3.8)$$

in which $p_h \in Q_h$ and $\bar{p}_h \in \bar{Q}_h$ are pressure fields and $\beta > 0$ is a parameter required for stability when using equal-order basis functions for the velocity components and pressure fields. When using a lower polynomial order for the pressure field relative to the velocity field it is possible to use $\beta = 0$ [11]. Penalization of the pressure jump was used by Hughes and Franca [12] to stabilize equal-order methods with discontinuous pressure for the Stokes equation, and by other authors for discontinuous Galerkin methods [13, 14]. However, different from Hughes and Franca [12], we add a non-dimensional unit viscosity to the term in the denominator to permit consideration

of the inviscid limit. Central in (3.8) is that the pressure-stabilizing term involves the difference between p_h and \bar{p}_h , rather than the jump in p_h across a facet as in other works [12, 13, 14]. Equation (3.7) is local in the sense that there is no direct interaction between p_h on neighboring cells. This is a key feature of the method with practical implications that will be elaborated upon in Section 6.

The numerical mass flux in (3.8) is not unique on cell facets; it can take on different values on different sides of a facet. This is in contrast with standard discontinuous Galerkin methods, in which the numerical mass flux is constructed such that it is uniquely defined on facets. A ‘global’ continuity equation is now furnished by insisting that the numerical mass flux $\hat{\mathbf{u}}_h$ be weakly continuous across cell facets, in that it satisfies

$$\sum_K \int_{\partial K} \hat{\mathbf{u}}_h \cdot \mathbf{n} \bar{q}_h \, ds - \int_{\partial\Omega} \bar{\mathbf{u}}_h \cdot \mathbf{n} \bar{q}_h \, ds = 0 \quad \forall \bar{q}_h \in \bar{Q}_h, \quad (3.9)$$

where $\bar{\mathbf{u}}_h \in \bar{V}_h$. Note that (3.9) implies that $\hat{\mathbf{u}}_h \cdot \mathbf{n} = \bar{\mathbf{u}}_h \cdot \mathbf{n}$ (weakly) on $\partial\Omega$.

3.2.2. Local/global momentum balance in conservative form. At time t and given the forcing term $\mathbf{f} \in [L^2(\mathcal{T})]^d$, the viscosity ν , the velocity $\bar{\mathbf{u}}_h \in \bar{V}_h$, and pressures $p_h \in Q_h$ and $\bar{p}_h \in \bar{Q}_h$, consider a Galerkin approximation $\mathbf{u}_h \in V_h$ that satisfies the following weak formulation of the momentum balance (2.1):

$$\begin{aligned} & \int_{\Omega} \frac{\partial \mathbf{u}_h}{\partial t} \cdot \mathbf{v}_h \, dx - \sum_K \int_K \boldsymbol{\sigma}_h : \nabla \mathbf{v}_h \, dx + \sum_K \int_{\partial K} \hat{\boldsymbol{\sigma}}_h \mathbf{n} \cdot \mathbf{v}_h \, ds \\ & + \sum_K \int_{\partial K} 2\nu (\bar{\mathbf{u}}_h - \mathbf{u}_h) \cdot \nabla^s \mathbf{v}_h \mathbf{n} \, ds = \int_{\Omega} \mathbf{f} \cdot \mathbf{v}_h \, dx \quad \forall \mathbf{v}_h \in V_h, \end{aligned} \quad (3.10)$$

where the momentum flux $\boldsymbol{\sigma}_h$ on cells is given by

$$\boldsymbol{\sigma}_h = \boldsymbol{\sigma}(\mathbf{u}_h, p_h) = p_h \mathbf{I} - 2\nu \nabla^s \mathbf{u}_h + \mathbf{u}_h \otimes \mathbf{u}_h, \quad (3.11)$$

and the ‘numerical’ momentum flux $\hat{\boldsymbol{\sigma}}_h$ on cell boundaries is given by

$$\hat{\boldsymbol{\sigma}}_h = \hat{\boldsymbol{\sigma}}_{a,h} + \hat{\boldsymbol{\sigma}}_{d,h}, \quad (3.12)$$

where the advective flux $\hat{\boldsymbol{\sigma}}_{a,h}$ is

$$\hat{\boldsymbol{\sigma}}_{a,h} = \hat{\boldsymbol{\sigma}}_a(\mathbf{u}_h, \bar{\mathbf{u}}_h, p_h, \bar{p}_h) = \mathbf{u}_h \otimes \hat{\mathbf{u}}_h + (\bar{\mathbf{u}}_h - \mathbf{u}_h) \otimes \lambda \hat{\mathbf{u}}_h, \quad (3.13)$$

in which $\hat{\mathbf{u}}_h$ is given by (3.8), λ is a function that takes on a value of either one or zero and is defined below, and the diffusive flux $\hat{\boldsymbol{\sigma}}_{d,h}$ is

$$\hat{\boldsymbol{\sigma}}_{d,h} = \hat{\boldsymbol{\sigma}}_d(\mathbf{u}_h, \bar{\mathbf{u}}_h, \bar{p}_h) = \bar{p}_h \mathbf{I} - 2\nu \nabla^s \mathbf{u}_h - \frac{\alpha}{h_K} 2\nu (\bar{\mathbf{u}}_h - \mathbf{u}_h) \otimes \mathbf{n}. \quad (3.14)$$

The function λ takes on a value of one on inflow cell boundaries (where $\hat{\mathbf{u}} \cdot \mathbf{n} < 0$), and takes on a value of zero on outflow cell boundaries (where $\hat{\mathbf{u}} \cdot \mathbf{n} \geq 0$). The formulation for the advective interface flux involves upwinding since $\hat{\boldsymbol{\sigma}}_a = \mathbf{u} \otimes \hat{\mathbf{u}}$ on outflow cell boundaries and $\hat{\boldsymbol{\sigma}}_a = \bar{\mathbf{u}} \otimes \hat{\mathbf{u}}$ on inflow cell boundaries. In (3.10), the fourth term on the left-hand side ensures symmetry of the diffusion operator (see Arnold et al. [15]). In (3.14), α is a penalty parameter, and such a term is typical of interior penalty methods. Just as for standard interior penalty methods, the role of the penalty term

in this context is to ensure stability, as detailed in Wells [5]. Equation (3.10) is ‘local’ in the sense that the weak momentum balance equation is posed cell-wise.

As with the numerical mass flux (3.8), the numerical momentum flux (3.12) is not single-valued on cell facets. A ‘global’ momentum balance equation is therefore formulated by insisting on continuity of the numerical flux $\hat{\boldsymbol{\sigma}}_h$ across element facets. This continuity constraint is imposed weakly by requiring that, for a given flux boundary condition $\mathbf{h} \in [L^2(\Gamma_N)]^d$,

$$\begin{aligned} \sum_K \int_{\partial K} \hat{\boldsymbol{\sigma}}_h \mathbf{n} \cdot \bar{\mathbf{v}}_h \, ds &= \int_{\Gamma_N} (1 - \lambda) (\bar{\mathbf{u}}_h \otimes \bar{\mathbf{u}}_h) \mathbf{n} \cdot \bar{\mathbf{v}}_h \, ds \\ &+ \int_{\Gamma_N} \mathbf{h} \cdot \bar{\mathbf{v}}_h \, ds \quad \forall \bar{\mathbf{v}}_h \in \bar{V}_h. \end{aligned} \quad (3.15)$$

The above equation implies that the numerical momentum flux $\hat{\boldsymbol{\sigma}}_h \mathbf{n}$ and the momentum flux on Γ_N , given by $\mathbf{h} + (1 - \lambda) (\bar{\mathbf{u}}_h \otimes \bar{\mathbf{u}}_h) \mathbf{n}$, coincide in a weak sense.

3.2.3. Local/global momentum balance in advective form. We now rephrase the conservative forms of the local and global momentum balance equations into advective formats with a view to formulating a skew-symmetric version of the advective terms.

Considering first the local momentum equation, substitution of the fluxes (3.11), (3.12) and (3.13) into (3.10) yields

$$\begin{aligned} \int_{\Omega} \frac{\partial \mathbf{u}_h}{\partial t} \cdot \mathbf{v}_h \, dx &- \sum_K \int_K \boldsymbol{\sigma}_{d,h} : \nabla \mathbf{v}_h \, dx - \sum_K \int_K (\mathbf{u}_h \otimes \mathbf{u}_h) : \nabla \mathbf{v}_h \, dx \\ &+ \sum_K \int_{\partial K} \hat{\boldsymbol{\sigma}}_{d,h} \mathbf{n} \cdot \mathbf{v}_h \, ds + \sum_K \int_{\partial K} (\hat{\mathbf{u}}_h \cdot \mathbf{n}) \mathbf{u}_h \cdot \mathbf{v}_h \, ds \\ &+ \sum_K \int_{\partial K} \lambda (\hat{\mathbf{u}}_h \cdot \mathbf{n}) (\bar{\mathbf{u}}_h - \mathbf{u}_h) \cdot \mathbf{v}_h \, ds \\ &+ \sum_K \int_{\partial K} 2\nu (\bar{\mathbf{u}}_h - \mathbf{u}_h) \cdot \nabla^s \mathbf{v}_h \mathbf{n} \, ds = \int_{\Omega} \mathbf{f} \cdot \mathbf{v}_h \, dx, \end{aligned} \quad (3.16)$$

in which $\boldsymbol{\sigma}_{d,h} = p_h \mathbf{I} - 2\nu \nabla^s \mathbf{u}_h$ is the diffusive flux on cells. Applying partial integration to the advective terms on K in (3.16),

$$\begin{aligned} \int_{\Omega} \frac{\partial \mathbf{u}_h}{\partial t} \cdot \mathbf{v}_h \, dx &- \sum_K \int_K \boldsymbol{\sigma}_{d,h} : \nabla \mathbf{v}_h \, dx + \sum_K \int_K (\nabla \mathbf{u}_h \mathbf{u}_h) \cdot \mathbf{v}_h \, dx \\ &+ \sum_K \int_K (\nabla \cdot \mathbf{u}_h) \mathbf{u}_h \cdot \mathbf{v}_h \, dx + \sum_K \int_{\partial K} ((\hat{\mathbf{u}}_h - \mathbf{u}_h) \cdot \mathbf{n}) \mathbf{u}_h \cdot \mathbf{v}_h \, ds \\ &+ \sum_K \int_{\partial K} \hat{\boldsymbol{\sigma}}_{d,h} \mathbf{n} \cdot \mathbf{v}_h \, ds + \sum_K \int_{\partial K} \lambda (\hat{\mathbf{u}}_h \cdot \mathbf{n}) (\bar{\mathbf{u}}_h - \mathbf{u}_h) \cdot \mathbf{v}_h \, ds \\ &+ \sum_K \int_{\partial K} 2\nu (\bar{\mathbf{u}}_h - \mathbf{u}_h) \cdot \nabla^s \mathbf{v}_h \mathbf{n} \, ds = \int_{\Omega} \mathbf{f} \cdot \mathbf{v}_h \, dx. \end{aligned} \quad (3.17)$$

We choose to discard the integrals involving $\nabla \cdot \mathbf{u}_h$ and $(\hat{\mathbf{u}}_h - \mathbf{u}_h) \cdot \mathbf{n}$, which by virtue of the continuity equation (3.7) and under an appropriate regularity assumption on

the exact solution will not disturb consistency of a Galerkin scheme (this will be addressed formally in Section 4). A reduced version of (3.17) now reads:

$$\begin{aligned} \int_{\Omega} \frac{\partial \mathbf{u}_h}{\partial t} \cdot \mathbf{v}_h \, dx + \sum_K \int_K (\nabla \mathbf{u}_h \mathbf{u}_h) \cdot \mathbf{v}_h \, dx - \sum_K \int_K \boldsymbol{\sigma}_{d,h} : \nabla \mathbf{v}_h \, dx \\ + \sum_K \int_{\partial K} \lambda (\hat{\mathbf{u}}_h \cdot \mathbf{n}) (\bar{\mathbf{u}}_h - \mathbf{u}_h) \cdot \mathbf{v}_h \, ds + \sum_K \int_{\partial K} \hat{\boldsymbol{\sigma}}_{d,h} \mathbf{n} \cdot \mathbf{v}_h \, ds \\ + \sum_K \int_{\partial K} 2\nu (\bar{\mathbf{u}}_h - \mathbf{u}_h) \cdot \nabla^s \mathbf{v}_h \mathbf{n} \, ds = \int_{\Omega} \mathbf{f} \cdot \mathbf{v}_h \, dx. \end{aligned} \quad (3.18)$$

Considering next the global momentum balance, inserting the expressions for the numerical flux (3.12) and (3.13) into the global flux continuity equation (3.15) yields,

$$\begin{aligned} \sum_K \int_{\partial K} \hat{\boldsymbol{\sigma}}_{d,h} \mathbf{n} \cdot \bar{\mathbf{v}}_h \, ds + \sum_K \int_{\partial K} (\hat{\mathbf{u}}_h \cdot \mathbf{n}) \mathbf{u}_h \cdot \bar{\mathbf{v}}_h \, ds \\ + \sum_K \int_{\partial K} \lambda (\hat{\mathbf{u}}_h \cdot \mathbf{n}) (\bar{\mathbf{u}}_h - \mathbf{u}_h) \cdot \bar{\mathbf{v}}_h \, ds \\ - \int_{\Gamma_N} (1 - \lambda) (\bar{\mathbf{u}}_h \cdot \mathbf{n}) \bar{\mathbf{u}}_h \cdot \bar{\mathbf{v}}_h \, ds = \int_{\Gamma_N} \mathbf{h} \cdot \bar{\mathbf{v}}_h \, ds. \end{aligned} \quad (3.19)$$

The second integral in (3.19) can be expanded as

$$\begin{aligned} \sum_K \int_{\partial K} (\hat{\mathbf{u}}_h \cdot \mathbf{n}) \mathbf{u}_h \cdot \bar{\mathbf{v}}_h \, ds = \sum_K \int_{\partial K} (\hat{\mathbf{u}}_h \cdot \mathbf{n}) (\mathbf{u}_h - \bar{\mathbf{u}}_h) \cdot \bar{\mathbf{v}}_h \, ds \\ + \sum_K \int_{\partial K} ((\hat{\mathbf{u}}_h - \bar{\mathbf{u}}_h) \cdot \mathbf{n}) \bar{\mathbf{u}}_h \cdot \bar{\mathbf{v}}_h \, ds + \int_{\partial \Omega} (\bar{\mathbf{u}}_h \cdot \mathbf{n}) \bar{\mathbf{u}}_h \cdot \bar{\mathbf{v}}_h \, ds, \end{aligned} \quad (3.20)$$

where we have used that $\bar{\mathbf{u}}_h$ is single-valued on cell facets, by definition. Discarding the term involving $(\hat{\mathbf{u}}_h - \bar{\mathbf{u}}_h) \cdot \mathbf{n}$, which is consistent with continuity equation (3.9), and substituting (3.20) into (3.19) leads to the following advective form of the global momentum equation:

$$\begin{aligned} \sum_K \int_{\partial K} \hat{\boldsymbol{\sigma}}_{d,h} \mathbf{n} \cdot \bar{\mathbf{v}}_h \, ds - \sum_K \int_{\partial K} (1 - \lambda) (\hat{\mathbf{u}}_h \cdot \mathbf{n}) (\bar{\mathbf{u}}_h - \mathbf{u}_h) \cdot \bar{\mathbf{v}}_h \, ds \\ + \int_{\Gamma_N} \lambda (\bar{\mathbf{u}}_h \cdot \mathbf{n}) \bar{\mathbf{u}}_h \cdot \bar{\mathbf{v}}_h \, ds = \int_{\Gamma_N} \mathbf{h} \cdot \bar{\mathbf{v}}_h \, ds, \end{aligned} \quad (3.21)$$

where we have taken into account that $\bar{\mathbf{v}}_h = \mathbf{0}$ on $\partial \Omega \setminus \Gamma_N$.

3.3. Semi-discrete finite element formulation. We define now a collection of functionals that together will define a complete finite element problem. For convenience, the notation $\mathbf{U} := (\mathbf{u}, \bar{\mathbf{u}}, p, \bar{p})$ will be used.

Based on the local continuity equation (3.7), we define the functional:

$$F_c(\mathbf{U}; q) := \sum_K \int_K \mathbf{u} \cdot \nabla q \, dx - \sum_K \int_{\partial K} \hat{\mathbf{u}} \cdot \mathbf{n} \, q \, ds, \quad (3.22)$$

where F_c is linear in q . Similarly, from the global continuity equation (3.9), the functional

$$\bar{F}_c(\mathbf{U}; \bar{q}) := \sum_K \int_{\partial K} \hat{\mathbf{u}} \cdot \mathbf{n} \bar{q} \, ds - \int_{\partial \Omega} \bar{\mathbf{u}} \cdot \mathbf{n} \bar{q} \, ds, \quad (3.23)$$

is defined, where \bar{F}_c is linear in \bar{q} . For the momentum equations, we define a local momentum balance functional that is a weighted combination of the local conservative balance (3.16) and the local advective balance (3.18):

$$\begin{aligned} F_m(\mathbf{U}; \mathbf{v}) &:= \int_{\Omega} \frac{\partial \mathbf{u}}{\partial t} \cdot \mathbf{v} \, dx - \chi \sum_K \int_K (\mathbf{u} \otimes \mathbf{u}) : \nabla \mathbf{v} \, dx \\ &+ (1 - \chi) \sum_K \int_K (\nabla \mathbf{u} \mathbf{u}) \cdot \mathbf{v} \, dx + \chi \sum_K \int_{\partial K} (\hat{\mathbf{u}} \cdot \mathbf{n}) \mathbf{u} \cdot \mathbf{v} \, ds \\ &+ \sum_K \int_{\partial K} \lambda (\hat{\mathbf{u}} \cdot \mathbf{n}) (\bar{\mathbf{u}} - \mathbf{u}) \cdot \mathbf{v} \, ds - \sum_K \int_K \boldsymbol{\sigma}_d : \nabla \mathbf{v} \, dx \\ &+ \sum_K \int_{\partial K} \hat{\boldsymbol{\sigma}}_d \mathbf{n} \cdot \mathbf{v} \, ds + \sum_K \int_{\partial K} 2\nu (\bar{\mathbf{u}} - \mathbf{u}) \cdot \nabla^s \mathbf{v} \mathbf{n} \, ds - \int_{\Omega} \mathbf{f} \cdot \mathbf{v} \, dx, \end{aligned} \quad (3.24)$$

where $\chi \in [0, 1]$ and F_m is linear in \mathbf{v} . In the same fashion, the global momentum flux continuity equations (3.19) and (3.21) are weighted and summed, leading to,

$$\begin{aligned} \bar{F}_m(\mathbf{U}; \bar{\mathbf{v}}) &:= \chi \sum_K \int_{\partial K} (\hat{\mathbf{u}} \cdot \mathbf{n}) \mathbf{u} \cdot \bar{\mathbf{v}} \, ds - (1 - \chi) \sum_K \int_{\partial K} (\hat{\mathbf{u}} \cdot \mathbf{n}) (\bar{\mathbf{u}} - \mathbf{u}) \cdot \bar{\mathbf{v}} \, ds \\ &+ \sum_K \int_{\partial K} \lambda (\hat{\mathbf{u}} \cdot \mathbf{n}) (\bar{\mathbf{u}} - \mathbf{u}) \cdot \bar{\mathbf{v}} \, ds + \sum_K \int_{\partial K} \hat{\boldsymbol{\sigma}}_d \mathbf{n} \cdot \bar{\mathbf{v}} \, ds \\ &- \int_{\Gamma_N} (\chi - \lambda) (\bar{\mathbf{u}} \cdot \mathbf{n}) \bar{\mathbf{u}} \cdot \bar{\mathbf{v}} \, ds - \int_{\Gamma_N} \mathbf{h} \cdot \bar{\mathbf{v}} \, ds, \end{aligned} \quad (3.25)$$

where \bar{F}_m is linear in $\bar{\mathbf{v}}$.

Defining now

$$F(\mathbf{U}; \mathbf{W}) := F_m(\mathbf{U}; \mathbf{v}) + \bar{F}_m(\mathbf{U}; \bar{\mathbf{v}}) + F_c(\mathbf{U}; q) + \bar{F}_c(\mathbf{U}; \bar{q}), \quad (3.26)$$

where $\mathbf{W} = (\mathbf{v}, \bar{\mathbf{v}}, q, \bar{q})$, a semi-discrete finite element problem at time t involves: given the forcing term $\mathbf{f} \in [L^2(\Omega)]^d$ the boundary condition $\mathbf{h} \in [L^2(\Gamma_N)]^d$ and the viscosity ν , find $\mathbf{U}_h \in V_h \times \bar{V}_h \times Q_h \times \bar{Q}_h$ such that

$$F(\mathbf{U}_h; \mathbf{W}_h) = 0 \quad \forall \mathbf{W}_h \in V_h \times \bar{V}_h \times Q_h \times \bar{Q}_h. \quad (3.27)$$

This completes the formulation of the semi-discrete finite element problem.

4. Properties of the semi-discrete formulation. We now demonstrate the consistency, mass conservation, momentum conservation and energy stability properties of the method for the semi-discrete formulation in (3.27). The presented results hold for the spaces \bar{V}_h and \bar{Q}_h , and deliberately also for the more restrictive case in which \bar{V}_h and \bar{Q}_h are replaced by \bar{V}_h^* and \bar{Q}_h^* , respectively, which we advocate in practice and will use in numerical examples.

PROPOSITION 4.1 (consistency). *If at a given time t , $\mathbf{u} \in (H^2(\Omega))^d$ and $p \in H^1(\Omega)$ solve equations (2.1)–(2.5), and $\bar{\mathbf{u}} = \gamma(\mathbf{u})$ and $\bar{p} = \gamma(p)$ on \mathcal{F} , where γ is a*

trace operator, then

$$F(\mathbf{U}; \mathbf{W}_h) = 0 \quad \forall \mathbf{W}_h \in V_h \times \bar{V}_h \times Q_h \times \bar{Q}_h, \quad (4.1)$$

for any $\chi \in [0, 1]$.

Proof. Considering first $\mathbf{v}_h = \mathbf{0}$, $\bar{\mathbf{v}}_h = \mathbf{0}$ and $\bar{q}_h = 0$, applying integration by parts to (4.1) leads to

$$\sum_K \int_K (\nabla \cdot \mathbf{u}) q_h \, dx - \sum_K \int_{\partial K} \frac{\beta h_K}{1 + \nu} (\bar{p} - p) q_h \, ds = 0 \quad \forall q_h \in Q_h, \quad (4.2)$$

which holds due to satisfaction of (2.3) and $\bar{p} = \gamma(p)$. Setting $\mathbf{v}_h = \mathbf{0}$, $\bar{\mathbf{v}}_h = \mathbf{0}$ and $q_h = 0$ in (4.1),

$$\sum_K \int_{\partial K \setminus \partial \Omega} \hat{\mathbf{u}} \cdot \mathbf{n} \bar{q}_h \, ds + \int_{\partial \Omega} \hat{\mathbf{u}} \cdot \mathbf{n} \bar{q}_h \, ds - \int_{\partial \Omega} \bar{\mathbf{u}} \cdot \mathbf{n} \bar{q}_h \, ds = 0 \quad \forall \bar{q}_h \in \bar{Q}_h, \quad (4.3)$$

which holds due to the regularity of \mathbf{u} and because $\hat{\mathbf{u}} = \gamma(\mathbf{u})$.

Setting $\bar{\mathbf{v}}_h = \mathbf{0}$, $q_h = 0$ and $\bar{q}_h = 0$ in (4.1) and applying integration by parts,

$$\begin{aligned} & \int_{\Omega} \left(\frac{\partial \mathbf{u}}{\partial t} + \nabla \cdot \boldsymbol{\sigma} - \mathbf{f} \right) \cdot \mathbf{v}_h \, dx - (1 - \chi) \int_{\Omega} (\nabla \cdot \mathbf{u}) \mathbf{u} \cdot \mathbf{v}_h \, dx \\ & + \chi \sum_K \int_{\partial K} ((\hat{\mathbf{u}} - \mathbf{u}) \cdot \mathbf{n}) \mathbf{u} \cdot \mathbf{v}_h \, ds + \sum_K \int_{\partial K} \lambda (\hat{\mathbf{u}} \cdot \mathbf{n}) (\bar{\mathbf{u}} - \mathbf{u}) \cdot \mathbf{v}_h \, ds \\ & + \sum_K \int_{\partial K} (\bar{p} - p) \mathbf{n} \cdot \mathbf{v}_h \, ds - \sum_K \int_{\partial K} \frac{\alpha}{h_K} 2\nu (\bar{\mathbf{u}} - \mathbf{u}) \otimes \mathbf{n} \cdot \mathbf{v}_h \, ds \\ & + \sum_K \int_{\partial K} 2\nu (\bar{\mathbf{u}} - \mathbf{u}) \cdot \nabla^s \mathbf{v}_h \mathbf{n} \, ds = 0 \quad \forall \mathbf{v}_h \in V_h, \end{aligned} \quad (4.4)$$

which holds due to \mathbf{u} and p satisfying equations (2.1) and (2.3), the regularity of \mathbf{u} and because $\bar{p} = \gamma(p)$ and $\bar{\mathbf{u}} = \hat{\mathbf{u}} = \gamma(\mathbf{u})$. Finally, setting $\mathbf{v}_h = \mathbf{0}$, $q_h = 0$ and $\bar{q}_h = 0$ in (4.1),

$$\begin{aligned} & \sum_K \int_{\partial K} \boldsymbol{\sigma} \mathbf{n} \cdot \bar{\mathbf{v}}_h \, ds + \sum_K \int_{\partial K} (\bar{p} - p) \mathbf{n} \cdot \bar{\mathbf{v}}_h \, ds - \sum_K \int_{\partial K} \frac{\alpha}{h_K} 2\nu (\bar{\mathbf{u}} - \mathbf{u}) \otimes \mathbf{n} \cdot \bar{\mathbf{v}}_h \, ds \\ & + \sum_K \int_{\partial K} ((\hat{\mathbf{u}} - \mathbf{u}) \cdot \mathbf{n}) \mathbf{u} \cdot \bar{\mathbf{v}}_h \, ds + \sum_K \int_{\partial K} \lambda (\hat{\mathbf{u}} \cdot \mathbf{n}) (\bar{\mathbf{u}} - \mathbf{u}) \cdot \bar{\mathbf{v}}_h \, ds \\ & - (1 - \chi) \sum_K \int_{\partial K} (\hat{\mathbf{u}} \cdot \mathbf{n}) \bar{\mathbf{u}} \cdot \bar{\mathbf{v}}_h \, ds - \int_{\Gamma_N} (\chi - \lambda) (\bar{\mathbf{u}} \cdot \mathbf{n}) \bar{\mathbf{u}} \cdot \bar{\mathbf{v}}_h \, ds \\ & = \int_{\Gamma_N} \mathbf{h} \cdot \bar{\mathbf{v}}_h \, ds \quad \forall \bar{\mathbf{v}}_h \in \bar{V}_h, \end{aligned} \quad (4.5)$$

which holds due to the regularity of \mathbf{u} , because $\bar{p} = \gamma(p)$ and $\bar{\mathbf{u}} = \hat{\mathbf{u}} = \gamma(\mathbf{u})$ and due to satisfaction of the flux boundary condition (2.5). Equation (4.1) follows from the summation of (4.2)–(4.5) and the linearity of F in \mathbf{v} , $\bar{\mathbf{v}}$, q and \bar{q} . \square

Key to the proof of Proposition 4.1 is the consistent formulation of the numerical fluxes, that is $\hat{\boldsymbol{\sigma}} = \boldsymbol{\sigma}$ and $\hat{\mathbf{u}} = \mathbf{u}$ if $\bar{\mathbf{u}} = \mathbf{u}$ and $\bar{p} = p$.

PROPOSITION 4.2 (mass conservation). *If \mathbf{u}_h and $\bar{\mathbf{u}}_h$ satisfy (3.27), then*

$$\int_{\partial K} \hat{\mathbf{u}}_h \cdot \mathbf{n} \, ds = 0 \quad \forall K \in \mathcal{T} \quad (4.6)$$

and

$$\int_{\partial\Omega} \bar{\mathbf{u}}_h \cdot \mathbf{n} \, ds = 0. \quad (4.7)$$

Proof. Setting $\mathbf{v}_h = \bar{\mathbf{v}}_h = \mathbf{0}$, $\bar{q}_h = 1$, and $q_h = 1$ on the cell K and $q_h = 0$ on $\mathcal{T} \setminus K$ leads to (4.6). Setting $\mathbf{v}_h = \bar{\mathbf{v}}_h = \mathbf{0}$ and $q_h = \bar{q}_h = 1$ in (3.27) leads to (4.7). \square

The local conservation property is in terms of the numerical mass flux $\hat{\mathbf{u}}$, as is typical for discontinuous Galerkin methods applied to Stokes flow [13, 14]. Classical local mass conservation would be satisfied if $\beta = 0$, but β must be greater than zero for stability of the equal-order case [12]. If the pressure field is chosen to be one polynomial order lower than the velocity field, then β can be set equal to zero and mass is conserved locally and exactly. However, it will be shown that reducing the size of the pressure space requires compromising on either momentum conservation or energy stability.

PROPOSITION 4.3 (momentum conservation). *If \mathbf{u}_h and $\bar{\mathbf{u}}_h$ solve (3.27), and the function spaces V_h, \bar{V}_h, Q_h and \bar{Q}_h are selected such that for a constant but otherwise arbitrary vector \mathbf{c} it holds that $\mathbf{v}_h \cdot \mathbf{c} \in Q_h \forall \mathbf{v}_h \in V_h$ and $\bar{\mathbf{v}}_h \cdot \mathbf{c} \in \bar{Q}_h \forall \bar{\mathbf{v}}_h \in \bar{V}_h$, then*

$$\frac{d}{dt} \int_K \mathbf{u}_h \, dx = \int_K \mathbf{f} \, dx - \int_{\partial K} \hat{\boldsymbol{\sigma}}_h \mathbf{n} \, ds \quad \forall K \in \mathcal{T}, \quad (4.8)$$

and if $\Gamma_D = \emptyset$

$$\frac{d}{dt} \int_{\Omega} \mathbf{u}_h \, dx = \int_{\Omega} \mathbf{f} \, dx - \int_{\partial\Omega} (1 - \lambda) (\bar{\mathbf{u}}_h \cdot \mathbf{n}) \bar{\mathbf{u}}_h \, ds - \int_{\partial\Omega} \mathbf{h} \, ds. \quad (4.9)$$

Proof. Setting $\mathbf{v}_h = \mathbf{e}_j$ and $q_h = -(1 - \chi) \mathbf{u}_h \cdot \mathbf{e}_j$ on K , where \mathbf{e}_j is a canonical unit basis vector, $\mathbf{v}_h = \mathbf{0}$ and $q_h = 0$ on $\mathcal{T} \setminus K$, $\bar{\mathbf{v}}_h = \mathbf{0}$ and $\bar{q}_h = 0$ in (3.27),

$$\begin{aligned} \frac{d}{dt} \int_K \mathbf{u}_h \cdot \mathbf{e}_j \, dx + \int_{\partial K} (\hat{\mathbf{u}}_h \cdot \mathbf{n}) \mathbf{u}_h \cdot \mathbf{e}_j \, ds + \int_{\partial K} \lambda (\hat{\mathbf{u}}_h \cdot \mathbf{n}) (\bar{\mathbf{u}}_h - \mathbf{u}_h) \cdot \mathbf{e}_j \, ds \\ + \int_{\partial K} \hat{\boldsymbol{\sigma}}_{d,h} \mathbf{n} \cdot \mathbf{e}_j \, ds = \int_K \mathbf{f} \cdot \mathbf{e}_j \, dx, \end{aligned} \quad (4.10)$$

which from the definition of the fluxes in equation (3.13) proves (4.8).

Setting $\mathbf{v}_h = \mathbf{e}_j$, $\bar{\mathbf{v}}_h = -\mathbf{e}_j$, $q_h = -(1 - \chi) \mathbf{u}_h \cdot \mathbf{e}_j$ and $\bar{q}_h = -(1 - \chi) \bar{\mathbf{u}}_h \cdot \mathbf{e}_j$ in (3.27) leads to (4.9) directly. \square

Local momentum conservation is in terms the numerical flux $\hat{\boldsymbol{\sigma}}_h$, as is a typical feature of discontinuous Galerkin methods. Note also the requirement on the size of the pressure space relative to the components of the velocity space, which would not be satisfied by methods that use lower-order polynomials for the pressure than for the velocity, such as Taylor–Hood elements. Such elements only conserve momentum when conservative forms of the momentum equation are used which, in the advective limit, requires compromising on energy stability. Provided that the requirements on the sizes of the function spaces are met, momentum conservation holds irrespective of the value of χ , i.e. for advective as well as conservative forms of the advection operator, and it will be shown that for $\chi = 1/2$ the method is also energy stable (see proposition 4.4).

For cases with Dirichlet boundary conditions ($\Gamma_D \neq \emptyset$), demonstration of momentum conservation is less straightforward since $\bar{\mathbf{v}}_h$ can not be set equal to \mathbf{e}_j on Γ_D .

This difficulty can be overcome by introducing auxiliary flux terms on Γ_D . Details of the approach can be found in Ref. [16].

PROPOSITION 4.4 (global energy stability). *If \mathbf{u}_h solves (3.27) with $\chi = 1/2$ and homogeneous boundary conditions, then in the absence of forcing terms and for a suitably large α*

$$\frac{d}{dt} \int_{\Omega} |\mathbf{u}_h|^2 dx \leq 0. \quad (4.11)$$

Proof. Setting $\mathbf{v}_h = \mathbf{u}_h$, $\bar{\mathbf{v}}_h = -\bar{\mathbf{u}}_h$, $q_h = -p_h$ and $\bar{q}_h = -\bar{p}_h$ in (3.27) gives, for $\chi = 1/2$,

$$\begin{aligned} & \int_{\Omega} \frac{\partial \mathbf{u}_h}{\partial t} \cdot \mathbf{u}_h dx + \sum_K \int_{\partial K} \left(\frac{1}{2} - \lambda \right) (\hat{\mathbf{u}}_h \cdot \mathbf{n}) |\bar{\mathbf{u}}_h - \mathbf{u}_h|^2 ds \\ & \quad - \sum_K \int_K \boldsymbol{\sigma}_{d,h} : \nabla \mathbf{u}_h dx - \sum_K \int_{\partial K} \hat{\boldsymbol{\sigma}}_{d,h} \mathbf{n} \cdot (\bar{\mathbf{u}}_h - \mathbf{u}_h) ds \\ & \quad + \sum_K \int_{\partial K} 2\nu (\bar{\mathbf{u}}_h - \mathbf{u}_h) \cdot \nabla^s \mathbf{u}_h \mathbf{n} ds + \int_{\Gamma_N} \left(\frac{1}{2} - \lambda \right) (\bar{\mathbf{u}}_h \cdot \mathbf{n}) |\bar{\mathbf{u}}_h|^2 ds \\ & \quad - \sum_K \int_K \mathbf{u}_h \cdot \nabla p_h dx - \sum_K \int_{\partial K} \hat{\mathbf{u}}_h \cdot \mathbf{n} (\bar{p}_h - p_h) ds + \int_{\partial \Omega} \bar{\mathbf{u}}_h \cdot \mathbf{n} \bar{p}_h ds = 0. \end{aligned} \quad (4.12)$$

Substituting the expressions for the diffusive fluxes given in (3.11) and (3.14) into the preceding equation,

$$\begin{aligned} & \int_{\Omega} \frac{1}{2} \frac{\partial |\mathbf{u}_h|^2}{\partial t} dx + \sum_K \int_{\partial K} \frac{1}{2} |\hat{\mathbf{u}}_h \cdot \mathbf{n}| |\bar{\mathbf{u}}_h - \mathbf{u}_h|^2 ds + \sum_K \int_K 2\nu |\nabla^s \mathbf{u}_h|^2 dx \\ & \quad + \sum_K \int_{\partial K} \frac{\alpha}{h_K} 2\nu |\bar{\mathbf{u}}_h - \mathbf{u}_h|^2 ds + 2 \sum_K \int_{\partial K} 2\nu (\bar{\mathbf{u}}_h - \mathbf{u}_h) \cdot \nabla^s \mathbf{u}_h \mathbf{n} ds \\ & \quad - \sum_K \int_K p_h \mathbf{I} : \nabla \mathbf{u}_h dx - \sum_K \int_{\partial K} \bar{p}_h \mathbf{n} \cdot (\bar{\mathbf{u}}_h - \mathbf{u}_h) ds + \int_{\Gamma_N} \frac{1}{2} |\bar{\mathbf{u}}_h \cdot \mathbf{n}| |\bar{\mathbf{u}}_h|^2 ds \\ & \quad - \sum_K \int_K \mathbf{u}_h \cdot \nabla p_h dx - \sum_K \int_{\partial K} \hat{\mathbf{u}}_h \cdot \mathbf{n} (\bar{p}_h - p_h) ds + \int_{\partial \Omega} \bar{\mathbf{u}}_h \cdot \mathbf{n} \bar{p}_h ds = 0, \end{aligned} \quad (4.13)$$

in which we have also used $(1/2 - \lambda) \mathbf{u} \cdot \mathbf{n} = |\mathbf{u} \cdot \mathbf{n}|/2$ on facets. After substitution of the mass flux $\hat{\mathbf{u}}_h$ given in (3.8) and the application of partial integration of the pressure gradient term, we finally obtain,

$$\begin{aligned} & \frac{d}{dt} \int_{\Omega} \frac{1}{2} |\mathbf{u}_h|^2 dx + \sum_K \int_{\partial K} \frac{1}{2} |\hat{\mathbf{u}}_h \cdot \mathbf{n}| |\bar{\mathbf{u}}_h - \mathbf{u}_h|^2 ds + \sum_K \int_K 2\nu |\nabla^s \mathbf{u}_h|^2 dx \\ & \quad + \sum_K \int_{\partial K} \frac{\alpha}{h_K} 2\nu |\bar{\mathbf{u}}_h - \mathbf{u}_h|^2 ds + 2 \sum_K \int_{\partial K} 2\nu (\bar{\mathbf{u}}_h - \mathbf{u}_h) \cdot \nabla^s \mathbf{u}_h \mathbf{n} ds \\ & \quad + \int_{\Gamma_N} \frac{1}{2} |\bar{\mathbf{u}}_h \cdot \mathbf{n}| |\bar{\mathbf{u}}_h|^2 ds + \sum_K \int_{\partial K} \frac{\beta h_K}{1 + \nu} |\bar{p}_h - p_h|^2 ds = 0. \end{aligned} \quad (4.14)$$

For the case $\nu = 0$, all terms in (4.14) other than the time derivative term, are guaranteed to be non-negative, and therefore (4.11) holds. For the case $\nu > 0$, no

conclusion as to the sign of $(\bar{\mathbf{u}}_h - \mathbf{u}_h) \cdot \nabla^s \mathbf{u}_h \mathbf{n}$ in (4.14) can be drawn. However, there exists an $\alpha > 0$, independent of h_K , such that (4.11) holds (see the proof in [5] for the diffusion equation). \square

The key to the energy stability is the use of the combined conservative/advective form of the momentum equations. The total kinetic energy in the method will decrease monotonically, despite \mathbf{u}_h not being point-wise divergence-free. The amount of dissipation is determined by the difference between the cell and facet velocity fields on facets $(\bar{\mathbf{u}}_h - \mathbf{u}_h)$ and the difference between the cell and facet pressure fields on facets $(\bar{p}_h - p_h)$. It is not possible to prove a cell-wise kinetic energy inequality.

Recall that the energy stable scheme is also momentum conserving if the dimensional components of the velocity space are subspaces of the pressure space (see Proposition 4.3). Otherwise, simultaneous momentum conservation ((4.8) and (4.9)) and energy stability (4.11) is not possible. Notably, this will be the case for finite element methods using lower-order polynomials for the pressure than for the velocity. For advection dominated flows such elements can only guarantee energy stability when compromising on momentum conservation or by adding artificial viscosity. In the viscous limit the requirement on the size of the velocity and pressure spaces can be relaxed without compromising energy stability, permitting a lower polynomial order for the pressure space than for the velocity space, which for Stokes flow is advantageous from the viewpoint of accuracy, as will be shown in Section 7.1.

A complete stability proof, for the Stokes case alone, would require a more subtle analysis, with the usual stability conditions demonstrated for suitably defined norms that include both functions on cells and the functions on facets. *A priori* stability and convergence estimates for the method applied to the advection-reaction-diffusion equation have been proved [5], and efforts in this direction for the Stokes equations are ongoing.

5. A fully-discrete formulation. We now present a fully-discrete formulation. The time interval of interest, I , is partitioned such that $I = (0, t_1, \dots, t_{N-1}, t_N]$ and time increments are denoted $\delta t_n = t_{n+1} - t_n$. We consider a θ -method for dealing with the time derivative, with mid-point values of a function y given by

$$y_{n+\theta} := (1 - \theta) y_n + \theta y_{n+1}, \quad (5.1)$$

where $\theta \in [0, 1]$ is a parameter.

The advective velocity will be evaluated at the current time t_n , thereby linearizing the problem (Picard linearization). For the momentum-related F -functionals presented in Section 3.3, we now present time-discrete counterparts. The term λ is always evaluated on the basis of the known velocity field at time t_n . A time-discrete

counterpart of (3.24) reads

$$\begin{aligned}
F_{\delta t, m}(\mathbf{U}_{n+1}; \mathbf{v}) &:= \int_{\Omega} \frac{\mathbf{u}_{n+1} - \mathbf{u}_n}{\delta t} \cdot \mathbf{v} \, dx - \chi \sum_K \int_K (\mathbf{u}_{n+\theta} \otimes \mathbf{u}_n) : \nabla \mathbf{v} \, dx \\
&+ (1 - \chi) \sum_K \int_K (\nabla \mathbf{u}_{n+\theta} \mathbf{u}_n) \cdot \mathbf{v} \, dx + \chi \sum_K \int_{\partial K} (\hat{\mathbf{u}}_n \cdot \mathbf{n}) \mathbf{u}_{n+\theta} \cdot \mathbf{v} \, ds \\
&+ \sum_K \int_{\partial K} \lambda (\hat{\mathbf{u}}_n \cdot \mathbf{n}) (\bar{\mathbf{u}}_{n+\theta} - \mathbf{u}_{n+\theta}) \cdot \mathbf{v} \, ds - \sum_K \int_K \boldsymbol{\sigma}_{d, n+\theta} : \nabla \mathbf{v} \, dx \\
&+ \sum_K \int_{\partial K} \hat{\boldsymbol{\sigma}}_{d, n+\theta} \mathbf{n} \cdot \mathbf{v} \, ds + \sum_K \int_{\partial K} 2\nu (\bar{\mathbf{u}}_{n+\theta} - \mathbf{u}_{n+\theta}) \cdot \nabla^s \mathbf{v} \, ds \\
&- \int_{\Omega} \mathbf{f}_{n+\theta} \cdot \mathbf{v} \, dx, \quad (5.2)
\end{aligned}$$

and a time-discrete counterpart of (3.25) reads

$$\begin{aligned}
\bar{F}_{\delta t, m}(\mathbf{U}_{n+1}; \bar{\mathbf{v}}) &:= \chi \sum_K \int_{\partial K} (\hat{\mathbf{u}}_n \cdot \mathbf{n}) \mathbf{u}_{n+\theta} \cdot \bar{\mathbf{v}} \, ds \\
&- (1 - \chi) \sum_K \int_{\partial K} (\hat{\mathbf{u}}_n \cdot \mathbf{n}) (\bar{\mathbf{u}}_{n+\theta} - \mathbf{u}_{n+\theta}) \cdot \bar{\mathbf{v}} \, ds \\
&+ \sum_K \int_{\partial K} \lambda (\hat{\mathbf{u}}_n \cdot \mathbf{n}) (\bar{\mathbf{u}}_{n+\theta} - \mathbf{u}_{n+\theta}) \cdot \bar{\mathbf{v}} \, ds + \sum_K \int_{\partial K} \hat{\boldsymbol{\sigma}}_{d, n+\theta} \mathbf{n} \cdot \bar{\mathbf{v}} \, ds \\
&- \int_{\Gamma_N} (\chi - \lambda) (\bar{\mathbf{u}}_n \cdot \mathbf{n}) \bar{\mathbf{u}}_{n+\theta} \cdot \bar{\mathbf{v}} \, ds - \int_{\Gamma_N} \mathbf{h}_{n+\theta} \cdot \bar{\mathbf{v}} \, ds. \quad (5.3)
\end{aligned}$$

Defining

$$\begin{aligned}
F_{\delta t}(\mathbf{U}_{n+1}; \mathbf{W}) &:= F_{\delta t, m}(\mathbf{U}_{n+1}; \mathbf{v}) \\
&+ \bar{F}_{\delta t, m}(\mathbf{U}_{n+1}; \bar{\mathbf{v}}) + F_c(\mathbf{U}_{n+1}; q) + \bar{F}_c(\mathbf{U}_{n+1}; \bar{q}), \quad (5.4)
\end{aligned}$$

a fully-discrete finite element problem at time t_{n+1} involves: given the solution $\mathbf{U}_{h, n} \in V_h \times \bar{V}_h \times Q_h \times \bar{Q}_h$ at time t_n , the forcing term $\mathbf{f}_{n+\theta} \in [L^2(\Omega)]^d$, the boundary condition $\mathbf{h}_{n+\theta} \in [L^2(\Gamma_N)]^d$ and the viscosity ν , find $\mathbf{U}_{h, n+1} \in V_h \times \bar{V}_h \times Q_h \times \bar{Q}_h$ such that

$$F_{\delta t}(\mathbf{U}_{h, n+1}; \mathbf{W}_h) = 0 \quad \forall \mathbf{W}_h \in V_h \times \bar{V}_h \times Q_h \times \bar{Q}_h. \quad (5.5)$$

For the scheme that has been adopted, $F_{\delta t}$ is linear in both $\mathbf{U}_{h, n+1}$ and \mathbf{W}_h .

We now demonstrate that the considered fully discrete formulation inherits the conservation and energy stability properties of the semi-discrete case. As for the semi-discrete case, all results hold if the spaces \bar{V}_h and \bar{Q}_h are replaced by \bar{V}_h^* and \bar{Q}_h^* , respectively.

PROPOSITION 5.1 (fully discrete mass conservation). *If $\mathbf{u}_{h, n+1}$ and $\bar{\mathbf{u}}_{h, n+1}$ satisfy (5.5), then*

$$\int_{\partial K} \hat{\mathbf{u}}_{h, n+1} \cdot \mathbf{n} \, ds = 0 \quad \forall K \in \mathcal{T}, \quad (5.6)$$

and

$$\int_{\partial\Omega} \bar{\mathbf{u}}_{h,n+1} \cdot \mathbf{n} \, ds = 0. \quad (5.7)$$

Proof. The proof follows the same steps as the proof of Proposition 4.2. \square

PROPOSITION 5.2 (fully discrete momentum conservation). *If $\mathbf{U}_{h,n}$ and $\mathbf{U}_{h,n+1}$ solve (5.5), and the function spaces V_h , \bar{V}_h , Q_h and \bar{Q}_h are selected such that for a constant but otherwise arbitrary vector \mathbf{c} it holds that $\mathbf{v}_h \cdot \mathbf{c} \in Q_h \forall \mathbf{v}_h \in V_h$ and $\bar{\mathbf{v}}_h \cdot \mathbf{c} \in \bar{Q}_h \forall \bar{\mathbf{v}}_h \in \bar{V}_h$, then*

$$\int_K \frac{\mathbf{u}_{h,n+1} - \mathbf{u}_{h,n}}{\delta t} \, dx = \int_K \mathbf{f}_{n+\theta} \, dx - \int_{\partial K} \hat{\boldsymbol{\sigma}}_{h,n+\theta} \mathbf{n} \, ds \quad \forall K \in \mathcal{T}, \quad (5.8)$$

and if $\Gamma_D = \emptyset$

$$\begin{aligned} \int_{\Omega} \frac{\mathbf{u}_{h,n+1} - \mathbf{u}_{h,n}}{\delta t} \, dx &= \int_{\Omega} \mathbf{f}_{n+\theta} \, dx \\ &\quad - \int_{\partial\Omega} (1-\lambda) (\bar{\mathbf{u}}_{h,n} \cdot \mathbf{n}) \bar{\mathbf{u}}_{h,n+\theta} \, ds - \int_{\partial\Omega} \mathbf{h}_{n+\theta} \, ds. \end{aligned} \quad (5.9)$$

Proof. The proof follows the same steps as the proof to Proposition 4.3. Equation (5.8) follows from setting $\mathbf{v}_h = \mathbf{e}_j$ and $q_h = -(1-\chi)\mathbf{u}_{h,n+\theta} \cdot \mathbf{e}_j$ on K , $\mathbf{v}_h = \mathbf{0}$ and $q_h = 0$ on $\mathcal{T} \setminus K$, $\bar{\mathbf{v}}_h = \mathbf{0}$ and $\bar{q}_h = 0$ in (5.5). Equation (5.9) follows from setting $\mathbf{v}_h = \mathbf{e}_j$, $\bar{\mathbf{v}}_h = -\mathbf{e}_j$, $q_h = -(1-\chi)\mathbf{u}_{h,n+\theta} \cdot \mathbf{e}_j$ and $\bar{q}_h = -(1-\chi)\bar{\mathbf{u}}_{h,n+\theta} \cdot \mathbf{e}_j$ in (5.5). \square

PROPOSITION 5.3 (fully discrete energy stability). *If $\mathbf{U}_{h,n}$ and $\mathbf{U}_{h,n+1}$ solve (5.5) with $\chi = 1/2$, $\mathbf{f} = \mathbf{0}$ and $\Gamma_D = \partial\Omega$, for $\theta \geq 1/2$ and suitably large α*

$$\int_{\Omega} |\mathbf{u}_{h,n+1}|^2 \, dx \leq \int_{\Omega} |\mathbf{u}_{h,n}|^2 \, dx. \quad (5.10)$$

Proof. For $\chi = 1/2$, setting $\mathbf{v}_h = \mathbf{u}_{h,n+\theta}$, $\bar{\mathbf{v}}_h = -\bar{\mathbf{u}}_{h,n+\theta}$, $q_h = -\theta p_{h,n+\theta}$ and $\bar{q}_h = -\theta \bar{p}_{h,n+\theta}$ in (5.5), and adding to (5.5) $F_c(\mathbf{U}_n; -(1-\theta)p_{n+\theta})$ and $\bar{F}_c(\mathbf{U}_n; -(1-\theta)p_{n+\theta})$,

$$\begin{aligned} &\int_{\Omega} \frac{\mathbf{u}_{h,n+1} - \mathbf{u}_{h,n}}{\delta t} \cdot \mathbf{u}_{h,n+\theta} \, dx + \sum_K \int_{\partial K} \left(\frac{1}{2} - \lambda \right) (\hat{\mathbf{u}}_{h,n} \cdot \mathbf{n}) |\bar{\mathbf{u}}_{h,n+\theta} - \mathbf{u}_{h,n+\theta}|^2 \, ds \\ &\quad - \sum_K \int_K \boldsymbol{\sigma}_{d,h,n+\theta} : \nabla \mathbf{u}_{h,n+\theta} \, dx - \sum_K \int_{\partial K} \hat{\boldsymbol{\sigma}}_{d,h,n+\theta} \mathbf{n} \cdot (\bar{\mathbf{u}}_{h,n+\theta} - \mathbf{u}_{h,n+\theta}) \, ds \\ &\quad + \sum_K \int_{\partial K} 2\nu (\bar{\mathbf{u}}_{h,n+\theta} - \mathbf{u}_{h,n+\theta}) \cdot \nabla^s \mathbf{u}_{h,n+\theta} \mathbf{n} \, ds \\ &\quad + \int_{\Gamma_N} \left(\frac{1}{2} - \lambda \right) (\bar{\mathbf{u}}_{h,n} \cdot \mathbf{n}) |\bar{\mathbf{u}}_{h,n+\theta}|^2 \, ds - \sum_K \int_K \mathbf{u}_{h,n+\theta} \cdot \nabla p_{h,n+\theta} \, dx \\ &\quad - \sum_K \int_{\partial K} \hat{\mathbf{u}}_{h,n+\theta} \cdot \mathbf{n} (\bar{p}_{h,n+\theta} - p_{h,n+\theta}) \, ds + \int_{\partial\Omega} \bar{\mathbf{u}}_{h,n+\theta} \cdot \mathbf{n} \bar{p}_{h,n+\theta} \, ds = 0. \end{aligned} \quad (5.11)$$

Taking into account that

$$\mathbf{u}_{h,n+\theta} = \delta t \left(\theta - \frac{1}{2} \right) \frac{\mathbf{u}_{h,n+1} - \mathbf{u}_{h,n}}{\delta t} + \frac{\mathbf{u}_{h,n+1} + \mathbf{u}_{h,n}}{2} \quad (5.12)$$

leads to

$$\int_{\Omega} \frac{\mathbf{u}_{h,n+1} - \mathbf{u}_{h,n}}{\delta t} \cdot \mathbf{u}_{h,n+\theta} \, dx = \left(\theta - \frac{1}{2} \right) \int_{\Omega} \frac{|\mathbf{u}_{h,n+1} - \mathbf{u}_{h,n}|^2}{\delta t} \, dx + \frac{1}{2} \int_{\Omega} \frac{|\mathbf{u}_{h,n+1}|^2}{\delta t} \, dx - \frac{1}{2} \int_{\Omega} \frac{|\mathbf{u}_{h,n}|^2}{\delta t} \, dx. \quad (5.13)$$

Following the same steps as in Proposition 4.4 proves that (5.10) holds when $\theta \geq 1/2$ and for sufficiently large α . \square

6. Algorithmic aspects. The fully-discrete finite element problem in (5.5) can lead to an efficient numerical implementation in which the functions on cells ($\mathbf{u}_{h,n+1}$ and $p_{h,n+1}$) are eliminated cell-wise in favor of the functions that live only on cell facets ($\bar{\mathbf{u}}_{h,n+1}$ and $\bar{p}_{h,n+1}$) via static condensation. Key to this algorithmic feature is that functions on cells are not linked directly across cell facets, in contrast with conventional discontinuous Galerkin methods. Rather, functions on neighboring cells communicate via the functions defined only on cell facets. Moreover, if the functions $\bar{\mathbf{u}}_h$ and \bar{p}_h are chosen to be continuous, the method will result in the same number of global degrees of freedom as for a continuous method on the same mesh (if interior degrees of freedom are eliminated from a continuous method via static condensation). Despite having the same number of global degrees of freedom as a continuous method, stabilizing mechanisms that are typical of discontinuous Galerkin methods are naturally incorporated. Moreover, for the advection-diffusion equation, it has been proved that the approach has the same stability properties as classical upwinded discontinuous Galerkin methods [5]. More detailed discussions on algorithmic aspects can be found in Refs. [1, 2].

7. Examples. We present now a number of examples in support of the analysis presented in the preceding sections. The computer code used to compute the examples presented in this section has been generated automatically from expressive input using tools from the FEniCS Project (<http://www.fenicsproject.org>) [17]. Specifically, an expressive domain-specific language for finite element variational statements in combination with automated code generation [18, 19, 20] and a programmable environment has been used [17]. The computer code used for all examples presented in this work is available under a GNU public license in the supporting material [10].

All examples use triangular elements, uniform partitionings and continuous facet functions, that is $\bar{\mathbf{u}}_h \in \bar{V}_h^*$ and $\bar{p}_h \in \bar{Q}_h^*$. When computing errors, analytical solutions which are polynomial are represented exactly. Otherwise analytical solutions are interpolated using eighth-order Lagrange basis functions on the same mesh. Exact quadrature is used in all cases.

7.1. Stokes flow with source. We consider a Stokes problem (by neglecting the momentum advection terms) with $\nu = 1$ on a unit square with $\mathbf{u} = \mathbf{0}$ on $\partial\Omega$. The source term \mathbf{f} is chosen such that the exact solution is:

$$\begin{aligned} u_x &= x^2 (1-x)^2 (2y - 6y^2 + 4y^3), \\ u_y &= -y^2 (1-y)^2 (2x - 6x^2 + 4x^3), \\ p &= x(1-x). \end{aligned} \quad (7.1)$$

The constraint $\int_{\Omega} p \, dx = 1/6$ is enforced by means of a Lagrange-multiplier, matching the solution in (7.1).

We investigate convergence rates in the L^2 -norm for the pressure and the velocity fields using equal-order polynomial elements ($k = \bar{k} = m = \bar{m}$). Polynomial orders ranging from one to five are considered. These results complement those presented in Labeur and Wells [1] for the same boundary-value problem, but in which the pressure field was continuous and only a polynomial order of one was considered. We set $\alpha = 6k^2$, based on observations for higher-order elements [5], and use $\beta = 10^{-4}$. The observed convergence behavior is presented in Figure 7.1. Standard convergence rates of order $k + 1$ for the velocity field and of order k for the pressure field are observed. The error in the divergence of the velocity field is examined via

$$e_{\text{div}} := \left(\sum_K \int_K (\nabla \cdot \mathbf{u})^2 dx \right)^{1/2}, \quad (7.2)$$

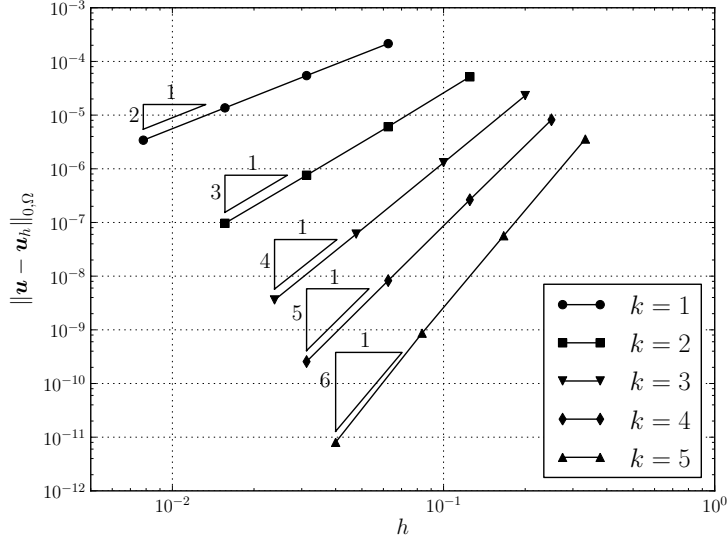
and the computed e_{div} is shown in Figure 7.2 for various polynomial orders and h -refinement. Clearly, the divergence error is small. For comparison, the divergence errors using the same method for the velocity field, but with a continuous pressure field [1] are shown in Figure 7.3. The observed convergence rates are similar to those for the discontinuous pressure case. However, particularly for the lower-order elements, the divergence error is significantly greater in the continuous pressure case.

For comparison, we consider a Taylor–Hood element with a continuous piecewise-quadratic velocity field and a continuous piecewise-linear pressure field, and an element constituted of a continuous piecewise-quadratic velocity field, enriched by cubic bubble functions, and a discontinuous piecewise-linear pressure field. The latter approach is referred to by some authors as the Crouzeix–Raviart method (e.g. [21, 22]), a convention that we adopt here. For our method we use corresponding polynomial orders of $k = \bar{k} = 2$ for the velocity and $m = \bar{m} = 1$ for the pressure and penalty parameters $\alpha = 6k^2$ and $\beta = 0$. Recall that it is permitted to use $\beta = 0$ in this case since the polynomial degree of the pressure field is lower than the polynomial degree of the velocity field, see Section 3.2.1. The observed convergence behavior is presented in Figure 7.4, which shows the expected convergence rates for the Taylor–Hood and Crouzeix–Raviart methods, and with the method formulated in this work showing the same rates, which are also the same as for the $k = \bar{k} = m = \bar{m} = 2$ case presented in Figure 7.1. The divergence error, measured by e_{div} , is shown in Figure 7.5. We note that while the Crouzeix–Raviart method conserves mass locally, the divergence error when measured in e_{div} is very close to that of the Taylor–Hood method, whereas for our method the divergence error is effectively zero.

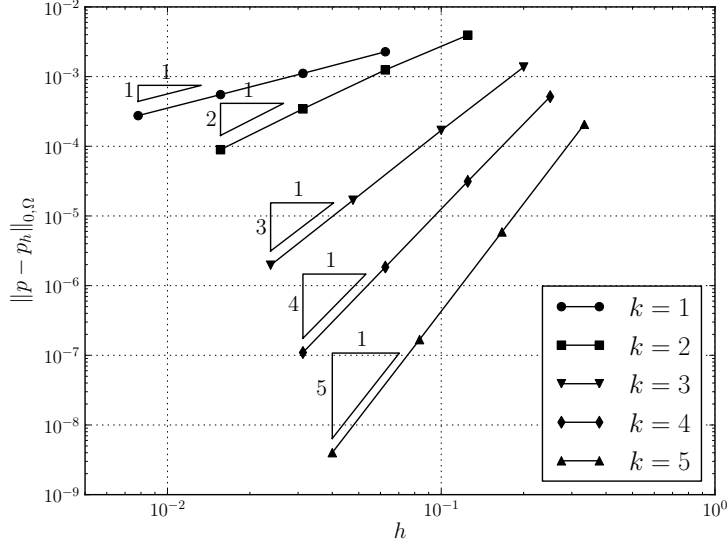
These convergence results demonstrate that in the viscous limit the equal-order pressure approximation is sub-optimal from the viewpoint of accuracy. However, in advection dominated flows the simultaneous satisfaction of Proposition 4.3 (momentum conservation) and Proposition 4.4 (energy stability) relies on a sufficiently rich pressure field relative to the velocity field, i.e. $k \leq m$, $\bar{k} \leq \bar{m}$, and consequently $\beta > 0$.

7.2. Kovasznay flow. We now consider the incompressible Navier–Stokes equations by examining the following analytical solution due to Kovasznay [23]:

$$\begin{aligned} u_x &= 1 - e^{\lambda x} \cos(2\pi y), \\ u_y &= \frac{\lambda}{2\pi} e^{\lambda x} \sin(2\pi y), \\ p &= \frac{1}{2} (1 - e^{2\lambda x}) + C, \end{aligned} \quad (7.3)$$



(a)



(b)

FIG. 7.1. Stokes flow: computed L^2 errors in (a) velocity and (b) pressure with h -refinement and for various polynomial orders k ($\alpha = 6k^2$ and $\beta = 10^{-4}$).

where C is an arbitrary constant and

$$\lambda = \frac{Re}{2} - \left(\frac{Re^2}{4} + 4\pi^2 \right)^{1/2}, \quad (7.4)$$

where Re is the Reynolds number. The solution represents laminar flow in the wake of a grid, see also [24, 25].

We use a rectangular domain $\Omega := \{(x, y) \in (-0.5, 1) \times (-0.5, 1.5)\}$. On $\partial\Omega$

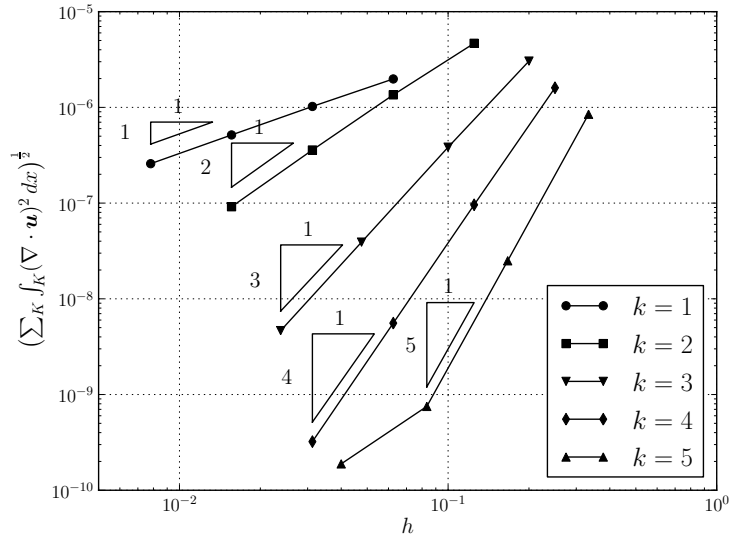


FIG. 7.2. Stokes flow with discontinuous pressure: divergence error with h -refinement and various polynomial orders k ($\alpha = 6k^2$ and $\beta = 10^{-4}$).

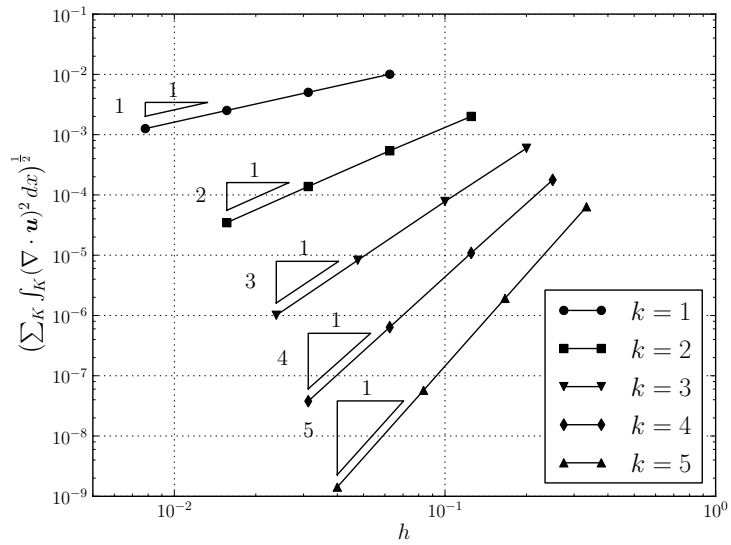
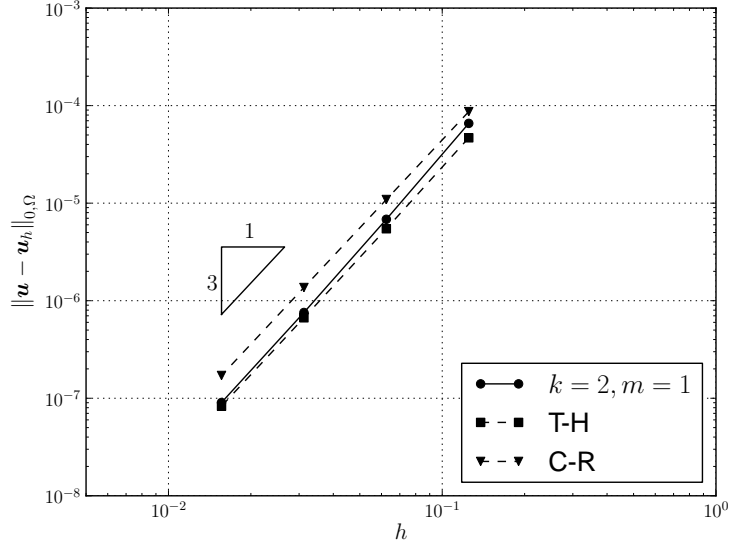
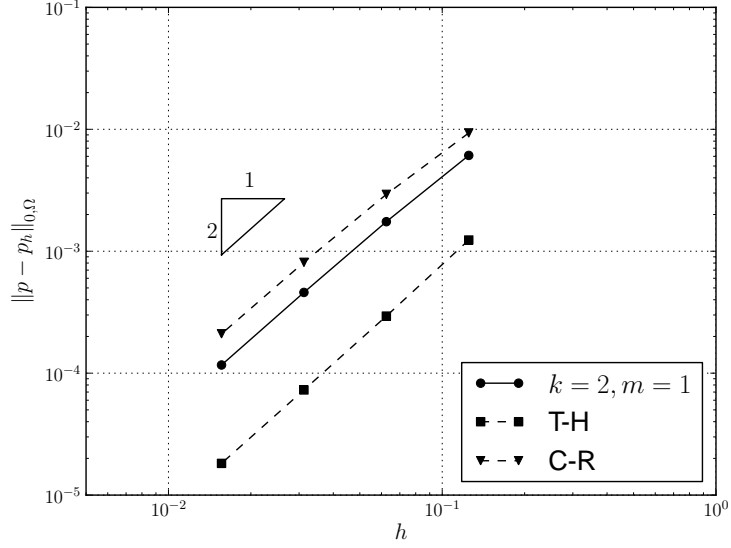


FIG. 7.3. Stokes flow with continuous pressure: divergence error with h -refinement and various polynomial orders k ($\alpha = 8k^2$).

Dirichlet boundary conditions for the velocity are specified according to equation (7.3). The pressure is prescribed in the lower-left corner of the domain. Equal-order polynomial elements are used ($k = \bar{k} = m = \bar{m}$) with polynomial orders ranging from one to five. The parameters $\chi = 1/2$, $\alpha = 6k^2$ and $\beta = 10^{-4}$ are used. We solve the



(a)



(b)

FIG. 7.4. Stokes flow: computed L^2 errors in (a) velocity and (b) pressure with h -refinement for polynomial orders $k = \bar{k} = 2$ and $m = \bar{m} = 1$ ($\alpha = 6k^2$ and $\beta = 0$), compared with Taylor–Hood (T-H) and Crouzeix–Raviart (C-R) methods.

stationary problem using a fixed point iteration with stopping criterion

$$\frac{|e_u^{i+1} - e_u^i|}{e_u^{i+1} + e_u^i} \leq \text{TOL}, \quad (7.5)$$

where e_u^i and e_u^{i+1} are the L^2 velocity error norms, relative to the exact solution, of the consecutive iterates i and $i + 1$, respectively, and TOL is a given tolerance which

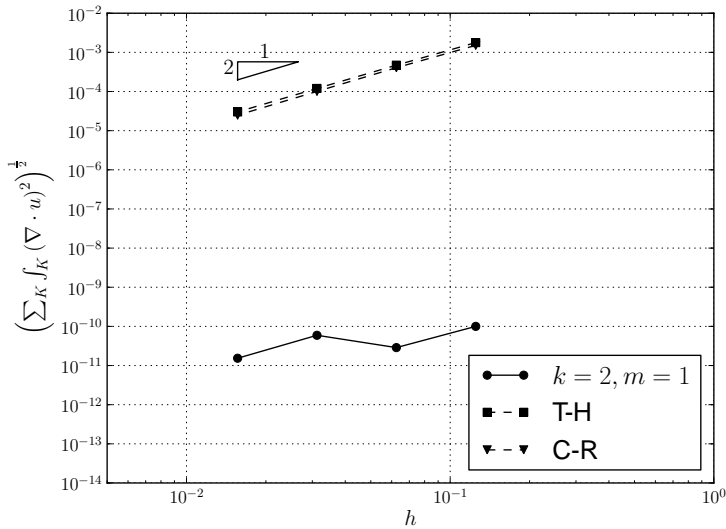


FIG. 7.5. Stokes flow: divergence error with h -refinement for polynomial orders $k = \bar{k} = 2$ and $m = \bar{m} = 1$ ($\alpha = 6k^2$ and $\beta = 0$), compared with Taylor–Hood (T-H) and Crouzeix–Raviart (C-R) methods.

is set to 10^{-4} .

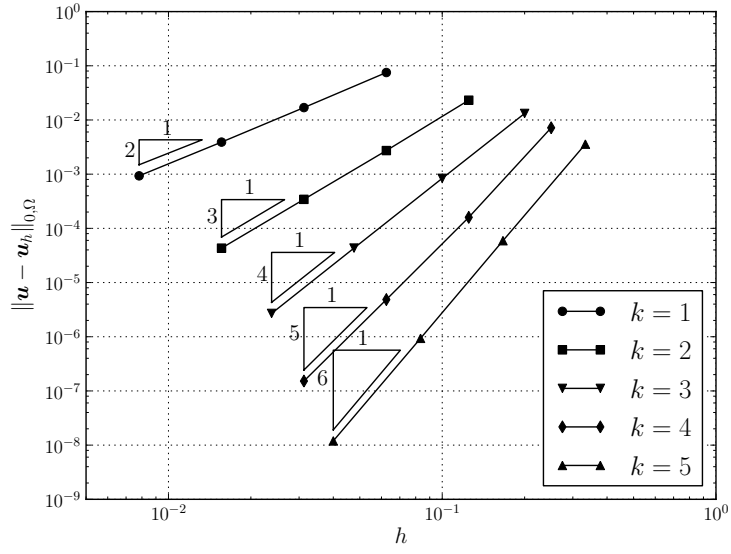
For $Re = 40$, the observed convergence rates in the L^2 -norm for the velocity and pressure fields are presented in Figure 7.6. Convergence rates of order $k + 1$ for the velocity field and of order k for the pressure field are observed. It was verified that these convergence results also hold for $\chi = 0$ (advective scheme) and $\chi = 1$ (conservative scheme).

7.3. Backward-facing step flow. The next example concerns stationary two-dimensional flow over a backward-facing step. Figure 7.7 presents the set-up of the problem. The step height S is equal to half the height of the main channel height D and the velocity profile in the inflow channel is parabolic with maximum velocity U_{\max} . Behind the step a recirculation zone develops with the re-attachment length x_ℓ depending on the Reynolds-number, as investigated experimentally by Armaly et al. [26]. The Reynolds number is defined as

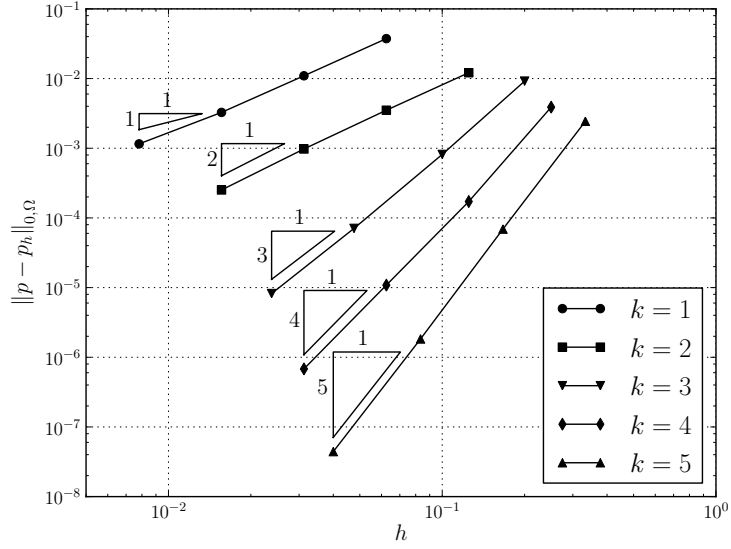
$$Re = \frac{UD}{\nu}, \quad (7.6)$$

where U is two-thirds of the maximum inflow velocity and ν is the kinematic viscosity [26].

The numerical test concerns the comparison of experimental and computed values of the dimensionless reattachment length x_ℓ/S [26]. We consider zero step length ($L = 0$), and a rectangular computational domain $\Omega := \{(x, y) \in (0, 15) \times (0, 1)\}$ which extends from the step over a length of 30 times the step height in the downstream direction. The domain is partitioned using 301 vertices in x -direction and 31 vertices in y -direction. On the left boundary ($x = 0$) the parabolic velocity profile with $U_{\max} = 1$ is imposed for $1/2 \leq y \leq 1$ using a Dirichlet boundary condition. Along the outflow boundary ($x = 15$) a homogeneous Neumann boundary condition for the velocity is used. On all other boundaries $\bar{\mathbf{u}} = \mathbf{0}$. The pressure degree of freedom for \bar{p} in the



(a)



(b)

FIG. 7.6. Kovasznay flow ($Re = 40$): computed L^2 errors in (a) velocity and (b) pressure with h -refinement and for various polynomial orders k ($\alpha = 6k^2$, $\beta = 10^{-4}$ and $\chi = 1/2$).

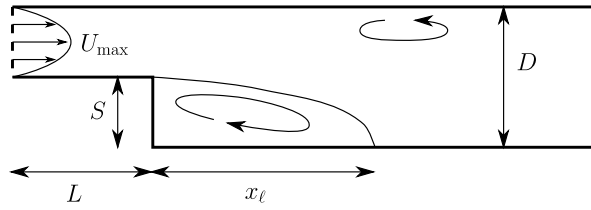


FIG. 7.7. Backward-facing step: general set-up.

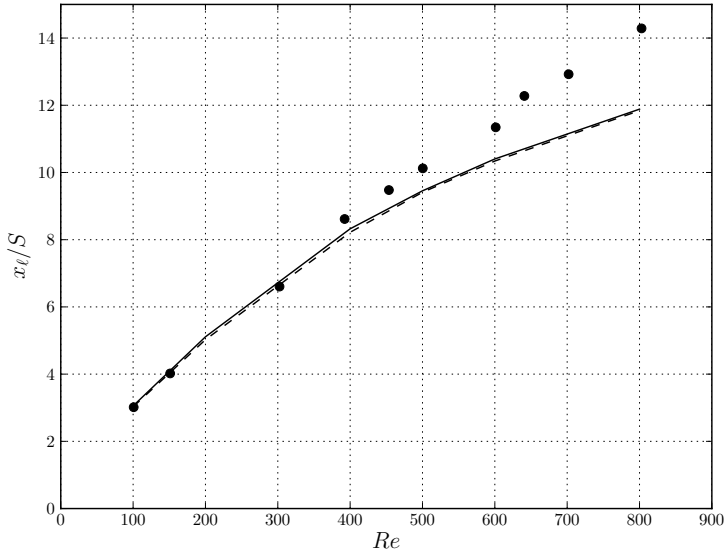


FIG. 7.8. *Backward-facing step: comparison of measured (●) and computed reattachment lengths for polynomial orders of $k = 1$ (solid) and $k = 2$ (dashed), experimental data from [26].*

lower-left corner of the domain is fixed. Using the definition in (7.6), the maximum inflow velocity and kinematic viscosity are adjusted to obtain a range of Reynolds numbers between 100 and 800. Equal order polynomials are used ($k = \bar{k} = m = \bar{m}$) with $k = 1$ and $k = 2$ considered. The parameters $\chi = 1/2$, $\alpha = 6k^2$ and $\beta = 10^{-4}$ are used. We solve the stationary problem using a fixed point iteration with a stopping criterion based on the L^2 -norm of the velocity,

$$\frac{\|\mathbf{u}_h\|_{0,\Omega}^{i+1} - \|\mathbf{u}_h\|_{0,\Omega}^i}{\|\mathbf{u}_h\|_{0,\Omega}^{i+1} + \|\mathbf{u}_h\|_{0,\Omega}^i} \leq \text{TOL}, \quad (7.7)$$

where i and $i + 1$ denote successive iterates and TOL is a tolerance, which is set to 10^{-6} .

The computed dimensionless reattachment lengths for various Reynolds numbers are presented in Figure 7.8, and are compared against measured data [26]. For $Re < 400$ the computed results are in good agreement with the results obtained from the experiments. For $Re > 400$ the computed results gradually deviate from the measurements, in a similar way as the results computed by Kim and Moin [27], and which can be attributed to the emergence of three-dimensional flow structures [26]. The computed streamlines for $Re = 800$ and polynomial orders of one are shown in Figure 7.9. The computed streamlines involve a secondary recirculation bubble which resides between dimensionless distances of 10.4 and 20.1 from the step, which is in good agreement with observed values of 11.2 and 19.6, respectively [26].

7.4. Chaotic advection. We now consider the energy stability properties of the method for the incompressible Navier–Stokes equations with $\chi = 1/2$. The incompressible Navier–Stokes equations are solved on the unit square with zero viscosity and boundary conditions $\mathbf{u} \cdot \mathbf{n} = 0$ and $\mathbf{h} \cdot \mathbf{s} = 0$ on $\partial\Omega$, where $\mathbf{s} \cdot \mathbf{n} = 0$. This corresponds to impermeable free-slip boundaries. The pressure is prescribed to be

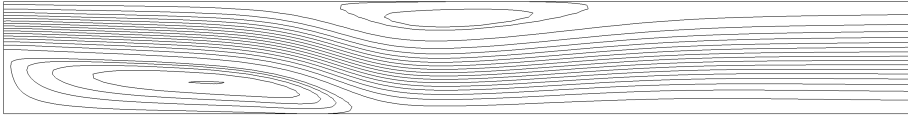


FIG. 7.9. Backward-facing step: computed streamlines for $Re = 800$ and $k = 1$, stream function intervals 0.2 (main flow), 0.005 (recirculation zone) and 0.002 (secondary bubble), respectively, figure stretched by a factor of two in the cross-stream direction.

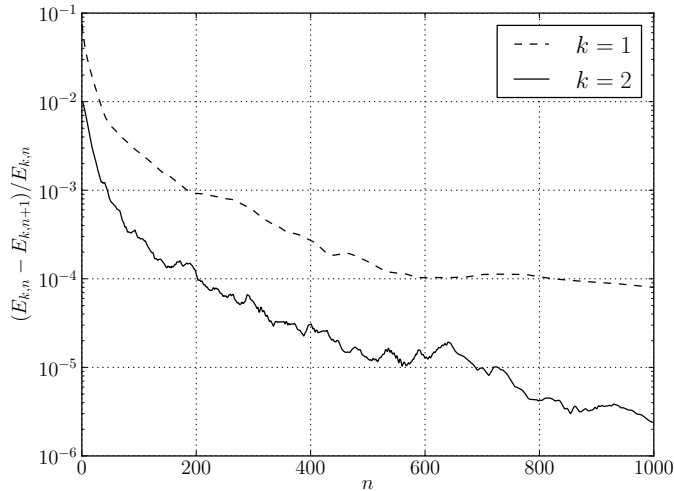


FIG. 7.10. Relative change in total kinetic energy between time steps for the incompressible Navier-Stokes test with $\chi = 1/2$, $\theta = 1/2$ and $\nu = 0$ for linear ($k = 1$) and quadratic ($k = 2$) elements. In both cases, a mesh with 32×32 vertices is used.

zero at a point in the domain. The initial condition $\mathbf{u}_0 = \mathbf{0}$ is used. A time step $\delta t = 0.2$ is adopted and the mesh has 32 cell vertices along each axis. To create a chaotic velocity field, in the first simulation step a random forcing term \mathbf{f} is used. Uniform random variables are generated at vertices such that for each component of the forcing vector $f_i \in [-1, 1]$. This field is then interpolated using linear Lagrange finite element basis functions. For the first step, $\nu = 1 \times 10^{-5}$, after which it is set to zero. This is done to start the simulation, since with $\mathbf{u}_0 = \mathbf{0}$, if $\nu = 0$ then (5.5) cannot be solved as the advective velocity at $t = 0$ is zero. For the first 5 time steps, a backward Euler scheme is used ($\theta = 1$) to damp oscillations due to the discontinuous nature of the forcing term. After the first 5 steps, $\theta = 1/2$ is used.

The relative change in the total kinetic energy between steps once $\theta = 1/2$ is presented in Figure 7.10 for the case of linear basis functions ($k = 1$) for all fields and the case of quadratic basis functions ($k = 2$) for all fields. Consistent with the analysis, the kinetic energy is observed to decrease monotonically. Not unexpectedly, the relative dissipation is smaller for the $k = 2$ case.

8. Conclusions. A generalization of a hybrid method that inherits attractive properties of continuous and discontinuous Galerkin methods has been presented and analyzed for the incompressible Navier-Stokes equations. The method incorporates

upwinding of the advective momentum flux naturally, it is observed to be stable for equal-order velocity/pressure basis functions and it has very good local mass conservation properties. These properties, usually associated with discontinuous Galerkin methods, can be achieved with the same number of global degrees of freedom as a continuous Galerkin method on the same mesh, thereby obviating the common criticism of discontinuous Galerkin methods that the number of degrees of freedom is too large compared to continuous methods. In contrast with our earlier work, the new formulation presented here involves a pressure field that is discontinuous across cell facets. This has implications for local mass conservation, which in the presented formulation is guaranteed in terms of the numerical flux. It is shown that with appropriately chosen (equal order) function spaces the method conserves momentum. Moreover, the new formulation presented in this work uses a skew-symmetric form of the momentum advection term. It has been shown that this, in combination with a suitable time integration scheme, guarantees that the global kinetic energy will decay monotonically, even if the velocity field is not point-wise divergence-free. The properties of the method that have been demonstrated by analysis are supported by numerical examples. Standard convergence rates for a range of polynomial orders are observed in the Stokes and Navier–Stokes examples, and simulations comparing the continuous and discontinuous pressure cases illustrate the advantage of discontinuous pressure fields for local mass conservation. The Navier–Stokes example concerning the flow over a backward facing step shows that the method performs well in an advection dominated case. The Navier–Stokes example concerning the evolution of a randomly generated velocity field demonstrates the energy decaying property of the skew-symmetric momentum advection term. The complete computer code for performing all presented numerical examples is made freely available under an open source license as part of the supporting material.

References.

- [1] R. J. Labeur and G. N. Wells. A Galerkin interface stabilisation method for the advection-diffusion and incompressible Navier-Stokes equations. *Comput. Methods Appl. Mech. Engrg.*, 196(49–52):4985–5000, 2007.
- [2] R. J. Labeur and G. N. Wells. Interface stabilised finite element method for moving domains and free-surface flows. *Comput. Methods Appl. Mech. Engrg.*, 198(5–8):615–630, 2009.
- [3] B. Cockburn, J. Gopalakrishnan, and R. Lazarov. Unified hybridization of discontinuous Galerkin, mixed, and continuous Galerkin methods for second order elliptic problems. *SIAM J. Numer. Anal.*, 47(2):1319–1365, 2009.
- [4] T. J. R. Hughes, G. Scovazzi, P. B. Bochev, and A. Buffa. A multiscale discontinuous Galerkin method with the computational structure of a continuous Galerkin method. *Comput. Methods Appl. Mech. Engrg.*, 195:2761–2787, 2006.
- [5] G. N. Wells. Analysis of an interface stabilised finite element method: The advection-diffusion-reaction equation. *SIAM J. Numer. Anal.*, 49(1):87–109, 2011.
- [6] B. Cockburn, B. Dong, J. Guzmán, M. Restelli, and R. Sacco. A hybridizable discontinuous Galerkin method for steady-state convection-diffusion-reaction problems. *SIAM J. Sci. Comput.*, 31(5):3827–3846, 2009.
- [7] N. C. Nguyen, J. Peraire, and B. Cockburn. A hybridizable discontinuous Galerkin method for Stokes flow. *Comput. Methods Appl. Mech. Engrg.*, 199(9–12):582 – 597, 2010.
- [8] H. Egger and J. Schöberl. A hybrid mixed discontinuous Galerkin finite-element

- method for convection-difusion problems. *IMA J. Numer. Anal.*, 30:1206–1234, 2010.
- [9] S. Güzey, B. Cockburn, and H. K. Stolarski. The embedded discontinuous Galerkin method: Application to linear shell problems. *Internat. J. Numer. Methods Engrg.*, 70:757–790, 2007.
 - [10] R. J. Labeur and G. N. Wells. Supporting material, 2012. URL <http://www.dspace.cam.ac.uk/handle/1810/241077>.
 - [11] P. Hansbo and M. G. Larson. Discontinuous Galerkin methods for incompressible and nearly incompressible elasticity by Nitsche’s method. *Comput. Methods Appl. Mech. Engrg.*, 191(17–18):1895–1908, 2002.
 - [12] T. J. R. Hughes and L. P. Franca. A new finite element formulation for computational fluid dynamics: VII. The Stokes problem with various well-posed boundary conditions: Symmetric formulations that converge for all velocity/pressure spaces. *Comput. Methods Appl. Mech. Engrg.*, 65(1):85–96, 1987.
 - [13] B. Cockburn, G. Kanschat, D. Schötzau, and Ch. Schwab. Local discontinuous Galerkin methods for the Stokes system. *SIAM J. Numer. Anal.*, 40(1):319–343, 2002.
 - [14] B. Cockburn, G. Kanschat, and Schötzau. An equal-order DG method for the incompressible Navier-Stokes equations. *J. Sci. Comput.*, 40:188–210, 2009.
 - [15] D. Arnold, F. Brezzi, B. Cockburn, and D. Marini. Unified analysis of discontinuous Galerkin methods for elliptic problems. *SIAM J. Numer. Anal.*, 39:1749–1779, 2002.
 - [16] T. J. R. Hughes and G. N. Wells. Conservation properties for the Galerkin and stabilised forms of the advection-diffusion and incompressible Navier-Stokes equations. *Comput. Methods Appl. Mech. Engrg.*, 194(9–11):1141–1159, 2005.
 - [17] A. Logg and G. N. Wells. DOLFIN: Automated finite element computing. *ACM Trans. Math. Software*, 37(2):20:1–20:28, 2010.
 - [18] R. C. Kirby and A. Logg. A compiler for variational forms. *ACM Trans. Math. Software*, 32(3):417–444, 2006.
 - [19] K. B. Ølgaard and G. N. Wells. Optimisations for quadrature representations of finite element tensors through automated code generation. *ACM Trans. Math. Software*, 37(1):8:1–8:23, 2010.
 - [20] K. B. Ølgaard, A. Logg, and G. N. Wells. Automated code generation for discontinuous Galerkin methods. *SIAM J. Sci. Comput.*, 31(2):849–864, 2008.
 - [21] P. M. Gresho, R. L. Sani, and M. S. Engelman. *Incompressible flow and the finite element method*. John Wiley and Sons, Chichester, 1998.
 - [22] H. C. Elman, D. J. Silvester, and A. J. Wathen. *Finite elements and fast iterative solvers with applications in incompressible fluid dynamics*. Oxford University Press, Oxford, 2005.
 - [23] L. Kovasznay. Laminar flow behind a two-dimensional grid. *Proceedings of the Cambridge Philosophical Society*, 44:58–62, 1948.
 - [24] R. M. Kirby and J. S. Spencer. Stabilization of spectral/hp element methods through spectral vanishing viscosity: Application to fluid mechanics modelling. *Comput. Methods Appl. Mech. Engrg.*, 195:3128–3144, 2006.
 - [25] T. Warburton, L. F. Pavarino, and J. S. Hesthaven. A pseudo-spectral scheme for the incompressible Navier-Stokes equations using unstructured nodal elements. *J. Comput. Phys.*, 164:1–21, 2000.
 - [26] B. F. Armaly, F. Durst, J. C. F. Pereira, and B. Schönung. Experimental and theoretical investigation of backward-facing step flow. *J. Fluid Mech.*, 127:473–

- 496, 1983.
- [27] J. Kim and P. Moin. Application of a fractional-step method to incompressible Navier-Stokes equations. *J. Comput. Phys.*, 59:308–323, 1985.